

# **Low Temperature Homodyne Detection of Pulsed Electron Spin Resonance Spectrometer**

A Project Report Submitted in Partial Fulfilment  
of the Requirements for the Degree of

**MASTERS OF SCIENCE**

by

**Sirswa Kuldeep Shree Ram**

(Roll No. 19MS156)

Department of Physical Sciences

**Student of**



**Indian Institute of Science Education and Research, Kolkata**

*Mohanpur, West Bengal, 741246, India*

Under the supervision of

**Prof. Chiranjib Mitra**

Department of Physical Sciences

**IISER Kolkata**

*May, 2024*

ঃ

---

## Declaration

I, Sirswa Kuldeep Shree Ram (**Roll No: 19MS156**), at this moment declare that the report included in this project entitled "**Low Temperature Homodyne Detection of Pulsed Electron Spin Resonance Spectrometer**," submitted to Indian Institute of Science Education and Research, Kolkata towards the partial requirement of **Masters of Science** in Physics genuinely carried out by me in the **Quantum Condensed Matter Lab and QIQT Lab, Department of Physical Sciences, IISER Kolkata**, India from August 2023 to May 2024 under the kind supervision of Prof. Chiranjib Mitra and has not formed the basis for the award of any degree or diploma, in this or any other institution or university.

In keeping with the general practice of reporting scientific observations, due acknowledgment has been made wherever the work described is based on the findings of other investigators.



May 17, 2024

Sirswa Kuldeep Shree Ram

IISER Kolkata

ঃ

---

# Certificate

It is certified that the research work included in the project report entitled “**Low Temperature Homodyne Detection of Pulsed Electron Spin Resonance Spectrometer,**” has been carried out by **Mr. Sirswa Kuldeep Shree Ram (Roll No. 19MS156)** under my supervision and guidance in **Quantum Condensed Matter Lab and QIQT Lab.** The content of this project report has not been submitted elsewhere for the award of any academic or professional degree.



May 17, 2024

IISER Kolkata

Prof. Chiranjib Mitra

Project Supervisor

ঃ

---

## Acknowledgements

I would like to extend my sincere gratitude toward my instructor and supervisor **Prof. Chiranjib Mitra**, for providing the opportunity to work on this project and for his valuable guidance in understanding this subject matter. I am grateful for his intellectual guidance, constant encouragement, valuable advice, and affection throughout the work. I am deeply indebted to **PMRF Anuvab Nandi** and **Kanav Sharma** for helping me with various difficulties throughout the entirety of this project. I would also like to thank Quantum Condensed Matter Lab and QIQT Lab members **Sandip Maity, Himadri Himani, Samiran Chakraborti, Sambhu Gopinath, Subhadip Manna, Projukta Das, Dr. Sayani Pal, Dr. Sumit Mukherjee, Sayan Chakraborty** for their help and support throughout this project. I am also very grateful to my family for being very supportive, especially throughout this project.



May 17, 2024

IISER Kolkata

Sirswa Kuldeep Shree Ram

ਸਾਹਿਬ

---

ਸਾਹਿਬ

To **Maa** (grandma), who raised me into who I am today.

Also, my Mom and Dad, along with all my relatives and friends,  
who helped in this journey called **LIFE**.

## Abstract

This thesis talks about the development of a pulsed electron spin resonance spectrometer from scratch, which can be used in quantum information processing. Rather than developing a traditional heterodyne setup, this thesis discusses the development of a homodyne setup. This thesis also talks about the development of a planar microwave resonator using simulation tools and fabrication methods. Details about resonators, their resonant frequency, ringdown time, dead time, and other microwave components have been covered. Free induction decay (FID) signals of the DPPH (2,2-diphenyl-1-picrylhydrazyl) sample have been measured at different temperatures. Their spin relaxation time is also measured. Attempted Rabi oscillations are also included in this thesis.



# Contents

<b>Declaration</b>	<b>2</b>
<b>Certificate</b>	<b>3</b>
<b>Acknowledgements</b>	<b>4</b>
<b>Dedication</b>	<b>5</b>
<b>Abstract</b>	<b>6</b>
<b>Contents</b>	<b>9</b>
<b>1 Introduction</b>	<b>10</b>
1.1 Why Electron Spin Resonance . . . . .	10
1.2 Structure of the thesis . . . . .	11
<b>2 Theory</b>	<b>12</b>
2.1 Magnetic Moment and Magnetic Field . . . . .	12
2.2 Magnetization of the System . . . . .	14
2.3 Microwave Magnetic Field . . . . .	16
2.4 The Rotating Frame . . . . .	17
2.5 Pulsed Electron Spin Resonance . . . . .	18
<b>3 Microwave Resonators</b>	<b>20</b>
3.1 Introduction . . . . .	20
3.2 Omega Resonator . . . . .	21
3.2.1 Geometry . . . . .	21
3.2.2 Simulation . . . . .	23



3.2.3	Fabrication Protocol . . . . .	25
3.3	Superconducting Resonator . . . . .	26
3.3.1	Reason for choosing YBCO Superconductor . . . . .	26
3.3.2	Geometry and Simulation . . . . .	27
3.3.3	Creation of YBCO Palette . . . . .	29
<b>4</b>	<b>Experimental Instruments</b>	<b>33</b>
4.1	Introduction . . . . .	33
4.2	Transmitter Circuit and its components . . . . .	33
4.2.1	RF Source (Vector Network Analyzer) . . . . .	34
4.2.2	Switch (first) . . . . .	35
4.2.3	Power Amplifier . . . . .	37
4.2.4	Isolator . . . . .	40
4.2.5	Switch (second) . . . . .	40
4.3	Central parts of the circuit . . . . .	41
4.3.1	Circulator . . . . .	41
4.3.2	Resonator . . . . .	43
4.3.3	Electromagnet and Cryostat . . . . .	44
4.3.4	Sample . . . . .	46
4.4	Receiver Circuit and its components . . . . .	46
4.4.1	Limiter . . . . .	47
4.4.2	Attenuator . . . . .	48
4.4.3	Switch (third) . . . . .	48
4.4.4	Low Noise Amplifiers and Attenuators . . . . .	49
4.4.5	Power Splitter . . . . .	51
4.4.6	LO Source (Signal Generator) . . . . .	52
4.4.7	Quadrature Power Splitter . . . . .	53



4.4.8	Frequency Mixer . . . . .	55
4.4.9	Low Pass Filter (LPF) . . . . .	56
4.4.10	Oscilloscope and Picoscope . . . . .	57
4.5	Complete Circuit . . . . .	58
<b>5</b>	<b>Data Processing and Results</b>	<b>61</b>
5.1	Omega Resonator and its characteristics . . . . .	61
5.2	CW ESR Sprectrum . . . . .	65
5.3	Pulsed ESR Circuit without Resonator . . . . .	68
5.4	Ringdown time and Deadtime . . . . .	69
5.5	FID signals of DPPH . . . . .	71
5.5.1	At Room Temperature . . . . .	73
5.5.2	At 270K Temperature . . . . .	73
5.5.3	At 180K Temperature . . . . .	73
5.6	Rabi Oscillation . . . . .	74
<b>6</b>	<b>Future Work</b>	<b>76</b>
<b>7</b>	<b>Conclusion</b>	<b>77</b>
	<b>Appendix A (Python Codes)</b>	<b>78</b>
	<b>References</b>	<b>86</b>

# Chapter 1

## 1 Introduction

### 1.1 Why Electron Spin Resonance

Electron spin resonance (ESR), also known as electron paramagnetic resonance, is a spectroscopic method to study materials with unpaired electrons [1]. These unpaired electrons have magnetic components  $m_s = \pm \frac{1}{2}$  and a spin quantum number  $s = \frac{1}{2}$ , and for this reason, electron spins are highly promising candidates for implementing qubits in quantum computing. Utilizing a magnetic field resolves the degeneracy of these spin states since the electron's magnetic moment will either align itself antiparallel (negative component) or parallel (positive component) with the applied magnetic field, creating a two-level system suitable for qubit operations. We employ rotations on the Bloch sphere to manipulate these qubits or use a single qubit gate to them, achieved through short but intense microwave pulses. This method is called pulsed ESR. This method applies gates to these qubits very quickly, in the order of nanoseconds. We worked with free radical DPPH (2,2-diphenyl-1-picrylhydrazyl), which has very short coherence times for our project. This report provides an overview of pulsed ESR theory, details about the simulation and fabrication done to develop a planar microwave resonator, and details about the construction of a custom experimental setup.

Rather than using the traditional X-band (8–12 GHz) frequency for ESR [13], [6], other frequencies such as Q-band ( $\sim$ 30 GHz), W-band ( $\sim$ 90 GHz), C-band (4–8 GHz), S-band (3–4 GHz), and L-band (1–2 GHz) can be used as

ESR spectrometer frequencies. However, this report will use the S-band frequency for the ESR signal. We will simulate and fabricate the desired resonator according to the requirements of our ESR signal, as stated above.

## 1.2 Structure of the thesis

In this thesis, Chapter 2 covers the theory, which includes the background and motivation for doing this experimentation and the theoretical aspects of the same. Later, Chapter 3 discusses the development of microwave resonators, specifically omega resonators and YBCO resonators. Chapter 4 covers a circuit diagram of the pulsed ESR setup and a summary of each component used in the circuit. Chapter 5 talks about data processing and recording the results. First, we will record the S11 result at different temperatures and then do the CW ESR. Afterward, we also calculated the ringdown time and dead time. We then recorded FID signals for DPPH at room temperature, 270K, and 180K. We also attempted Rabi oscillation at these temperatures. Chapter 6 talks about the future work that can be done, and chapter 7 concludes my thesis.

## Chapter 2

## 2 Theory

### 2.1 Magnetic Moment and Magnetic Field

If a static magnetic field ( $B_0$ ) is applied to an electron, the degeneracy of the magnetic spin levels is resolved. So, it will create a two-level system with specific energy due to the Zeeman effect. It can be seen in Figure 1.

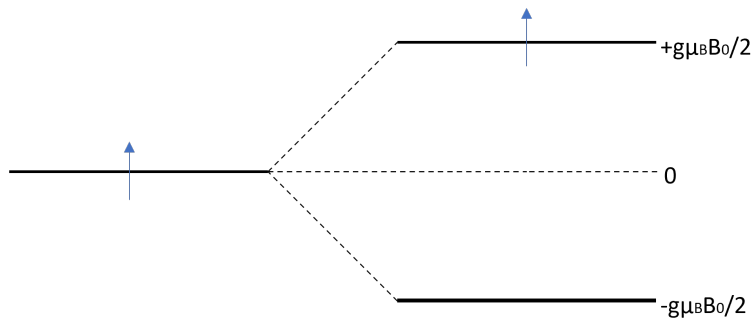


Figure 1: Zeeman splitting

Two essential parameters used are the constant magnetic field ( $\vec{B}_0$ ) and the excitation frequency ( $\nu$ ). We will keep the frequency (microwave) constant but change the field to get the required ESR signal. If the direction of the magnetic field aligns with the z-direction,  $\vec{B}_0 = B_0 \hat{k}$ , then the Hamiltonian describing the interaction between the field and the spin can be:

$$\hat{H}_0 = -\hat{\mu} \cdot \vec{B}_0 = -\hat{\mu}_z B_0$$

$$\hat{H}_0 = -\gamma \hat{S}_z B_0$$

From this equation, it can be said that the eigenstates of  $\hat{H}_0$  are identical to

those of  $\hat{S}_z$ . So, the corresponding eigenvalues will be:

$$\hat{H}_0 |\pm \frac{1}{2}\rangle = \mp \frac{1}{2} \hbar \gamma B_0 |\pm \frac{1}{2}\rangle = E_{\pm} |\pm \frac{1}{2}\rangle$$

So the energy gap will be:

$$\Delta E = g\mu_B B_0 = h\nu$$

When this energy gap and electromagnetic waves are in resonance (i.e.,  $\omega = -\gamma B_0$ ), we observe the absorption of these waves, which we call ESR. So, the time evolution of the dipole moment in the above Heisenberg picture is:

$$\begin{aligned} \frac{d\hat{\vec{\mu}}}{dt} &= \frac{i}{\hbar} [\hat{H}_0, \hat{\vec{\mu}}] = -\frac{i}{\hbar} \left[ \sum_i \hat{\mu}_i B_{0i}, \hat{\vec{\mu}} \right] \\ \frac{d\hat{\vec{\mu}}}{dt} &= -\frac{i}{\hbar} \sum_i B_{0i} [\hat{\mu}_i, \hat{\vec{\mu}}] = -\frac{i}{\hbar} \sum_i B_{0i} \gamma^2 [\hat{S}_i, \hat{\vec{\mu}}] \\ \frac{d\hat{\vec{\mu}}}{dt} &= -\frac{i}{\hbar} \sum_i \sum_j B_{0i} \gamma^2 i \hbar \epsilon_{ijk} \hat{S}_j = -\frac{i}{\hbar} \gamma i \hbar \sum_i \sum_j B_{0i} \epsilon_{ijk} \hat{\mu}_j \\ \frac{d\hat{\vec{\mu}}}{dt} &= \gamma \hat{\vec{\mu}} \times \vec{B}_0 \\ \implies \frac{d\vec{\mu}}{dt} &= \gamma \vec{\mu} \times \vec{B}_0 \end{aligned}$$

Using this equation, we can show the accuracy of the magnetic moment around the field at frequency  $\omega_L = -\gamma B_0$  (Figure 2). This is Larmor precession, and  $\omega_L$  is Larmor frequency.

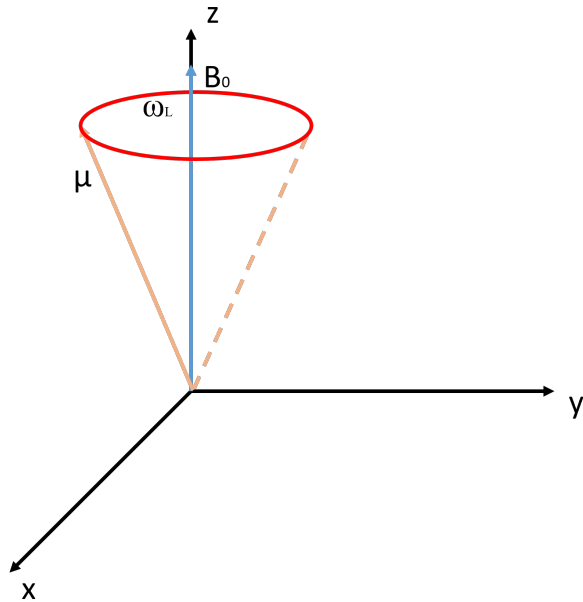


Figure 2: Larmor Precession

## 2.2 Magnetization of the System

When working in the real world, it is not easy to work with a single electron; instead, we will work with an ensemble of electrons. So we cannot simply talk about the magnetic moment of individual electrons but instead about the magnetization of the system, which can be given as:

$$\vec{M} = \frac{\sum \vec{\mu}}{V}$$

So, the time evolution of the magnetization in the above Heisenberg picture can be written as:

$$\frac{d\vec{M}}{dt} = \gamma \vec{M} \times \vec{B}_0$$

From the above equation, it is clear that Larmor precession also works for magnetization. In the ideal case, it should persist indefinitely, but in equilibrium,

the magnetization will invariably be aligned with the applied magnetic field (i.e., along the z-axis). So, rather than the Larmor precession, it will follow a damped precession due to spin interactions and environmental influences. To accurately capture the magnetization dynamics, we will follow the below Bloch equation (assuming  $\vec{B}$  constant and  $\vec{M}(0)$  as initial magnetization):

$$\frac{d\vec{M}}{dt} = \gamma \vec{B} \times \vec{M} - \frac{M_x}{T_2} \hat{i} - \frac{M_y}{T_2} \hat{j} - \frac{M_0 - M_z}{T_1} \hat{k}$$

So the solution to the above equation is:

$$M_x(t) = [M_x(0)\cos\omega_0 t + M_y(0)\sin\omega_0 t]e^{-\frac{t}{T_2}}$$

$$M_y(t) = [M_y(0)\cos\omega_0 t - M_x(0)\sin\omega_0 t]e^{-\frac{t}{T_2}}$$

$$M_z(t) = M_z(0)e^{-\frac{t}{T_1}} + M_0[1 - e^{-\frac{t}{T_1}}]$$

From the above equation, we can see that the magnetization is not conserved. So, it changes differently in the longitudinal (along the magnetic field) and transverse (normal to the magnetic field) directions with respect to time. This can be explained by the electron spin interactions with the phonons, dominating the relaxation along the magnetic field and the electron dipolar interactions, dominating the relaxation normal to the magnetic field. So, it can be concluded that the magnetization will initially be on the Bloch sphere's surface. Then, it will go inside during the dynamics, finally reaching equilibrium along the magnetic field on the surface of the Bloch sphere. This can be seen in Figure 3.

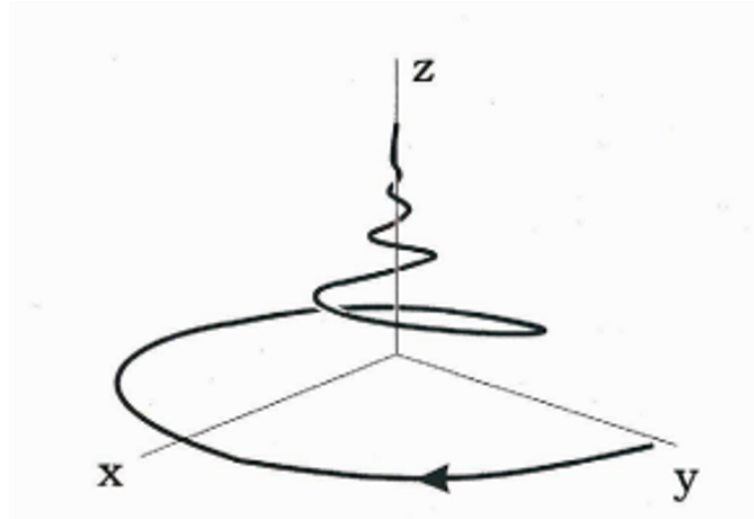


Figure 3: Magnetization Dynamics [7]

### 2.3 Microwave Magnetic Field

To investigate the magnetization dynamics further, we first need to disturb the existing equilibrium, i.e., take the magnetization far from the direction along the magnetic field. This is generally done by applying a time-dependent magnetic field along the direction perpendicular to the constant magnetic field ( $B_0$ ) with frequency  $\omega$ . This time-dependent magnetic field, also known as a microwave field, forces changes in electron spin states. The applied microwave field (assuming along the y-axis) is the combination of two rotating magnetic fields moving in opposite directions at the same frequency. So, it can be written as:

$$\vec{B}_m = [B_1 \sin \omega t \hat{i} + B_1 \cos \omega t \hat{j}] - [B_1 \sin \omega t \hat{i} - B_1 \cos \omega t \hat{j}]$$

$$\vec{B}_m = 2B_1 \cos \omega t \hat{j}$$

So, the total magnetic field will be:

$$\vec{B}_t = B_0 \hat{k} + 2B_1 \cos\omega t \hat{j}$$

## 2.4 The Rotating Frame

After applying a microwave field, the total magnetic field changes as given above, so the Hamiltonian of this new total magnetic field for the electron interaction is:

$$\hat{H}_0 = -\gamma \hat{S}_z B_0 - 2\gamma \hat{S}_y B_1 \cos\omega t$$

We can see that this Hamiltonian is time-dependent, so we will go into the rotating frame itself to remove the time dependency on the Hamiltonian. We will apply the following transformation:

$$|\phi(t)\rangle = R(t)|\psi(t)\rangle$$

So, the Hamiltonian becomes:

$$\hat{H}'_0(t) = I\hbar \dot{R}(t)R(t)^\dagger + R(t)\hat{H}_0(t)R(t)^\dagger$$

If we consider  $R(t) = e^{-i\omega t \hat{S}_z}$  for the rotating frame at  $\omega$  (similar to that of Larmor precession), then on applying approximation of rotating wave, our Hamiltonian will become time-independent, as it can be seen here:

$$\hat{H}'_0 = -\gamma \hat{S}_z (B_0 + \frac{\omega}{\gamma}) - \gamma \hat{S}_y B_1 = -\gamma \hat{S} \cdot \vec{B}_e$$

So, the effective magnetic field will be:

$$\vec{B}_e = (B_0 - \frac{\omega}{|\gamma|})\hat{k} + B_1\hat{j}$$

## 2.5 Pulsed Electron Spin Resonance

The effective magnetic field we calculated is the principle equation of the pulsed ESR experiment. If the applied microwave pulse has a frequency equivalent to that of the Larmor frequency, i.e.,  $\omega = \omega_L = \gamma B_0$ , then in such cases, the z-component of the effective magnetic field vanishes. So, the new effective magnetic field [11], [2] will become:

$$\vec{B}_e = B_1\hat{j}$$

So, we can say that the time evolution of magnetization in the rotating frame shows that it will revolve around the y-axis since the effective magnetic field is along the y-axis. This can be seen in Figure 4.

So, the frequency of this spin precession is:

$$\omega_1 = \gamma B_1$$

If we control the pulse duration applied ( $t_1$ ), we can accurately get the desired rotation angle. So, the angle of rotation can be given by:

$$\theta = \gamma B_1 t_1$$

For example, if we want to create a  $\frac{\pi}{2}$  rotation of the spin state, then we will need to apply a  $\frac{\pi}{2}$  pulse. We can calculate the pulse length since we already have an angle of rotation.

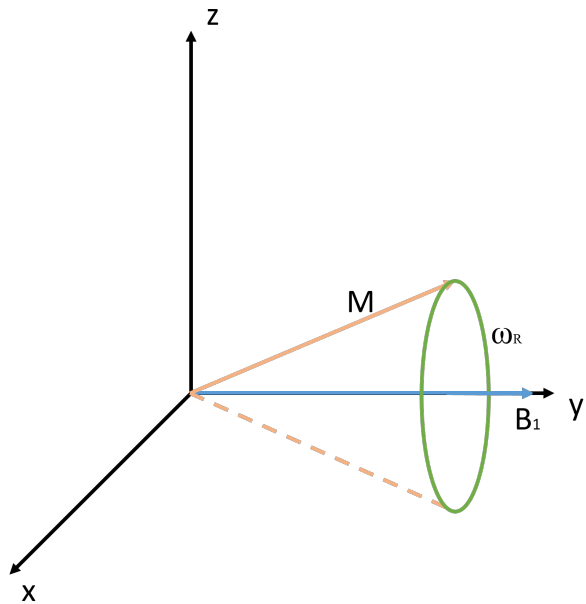


Figure 4: Spin precession at resonant irradiation in rotating frame

$$\gamma B_1 t_1 = \frac{\pi}{2}$$

## Chapter 3

# 3 Microwave Resonators

## 3.1 Introduction

Microwave resonators serve as interactive mediums between our pulsed electron spin resonance setup and the sample. So, it plays a crucial role in electron spin resonance spectrometers. So it provides microwaves to the sample generated by the vector network analyzer (VNA) through the transmitter circuit, then detects weak ESR signals from the sample and sends them to the receiver circuit, which delivers them to an oscilloscope or a picoscope. This procedure will be discussed in later chapters. This resonator is also responsible for amplifying the microwave pulse (field) for the sample kept on it.

When these resonators are excited by this microwave field (electromagnetic field), the capacitor and inductor components of the resonators store electric and magnetic energy, respectively. Consequently, after this microwave pulse is concluded, the resonators release the stored energy from the capacitor and inductor components, which then creates dead time for our system. This dead time made by a resonator is called the ring-down time of that resonator. It depends mainly on the quality factor (the Q factor), which depends on many factors, including the temperature at which pulsed electron spin resonance is carried out. The Q factor of any resonator at a given temperature can be calculated by:

$$\text{Quality Factor} = \frac{\text{Center Resonant Frequency}}{3dB \text{ Bandwidth}}$$

Resonators also enhances weak ESR signals depending on Q factor of the resonator, i.e., the higher the Q factor, the greater the signal strength. However, we also know that a high Q factor leads to a very high dead time, i.e., ring downtime. So, in the case of pulsed electron spin resonance, a generally low Q factor is preferred but should be high enough to get a good ESR signal that can be detected above the noise floor. Therefore, planar resonators, which have a loop gap, are preferred rather than cavity resonators because of their low-quality factor. Further, out of the many resonators created, we will discuss the omega resonator that was simulated and fabricated for our pulsed electron spin resonance experiments and introduce a YBCO superconducting resonator, which can also be used in future works.

## 3.2 Omega Resonator

### 3.2.1 Geometry

Our resonator has a central part of the dielectric substrate and a conducting plate on both sides. The side view of the omega resonator can be seen in Figure 5. In this diagram, the plate below, which is of height  $h$ , will act as a ground plane, the central blue part is a dielectric substrate, and the top part is the conducting surface. To better understand the structure, the top view of the omega resonator is given in Figure 6. In this diagram, we can see all the parameters of the resonator.  $s$  is the radius of the central gap of the omega, and  $t$  is the thickness of that omega structure. The line attached to the corner of the resonator is called the feedline, where we will attach a connector for calculations. The central part with  $\Omega$ -like structure is where we will keep our sample for measurement in later experiments.

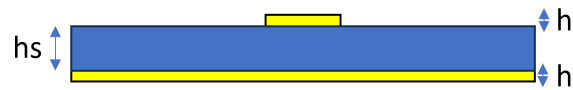


Figure 5: Side view of Omega Resonator

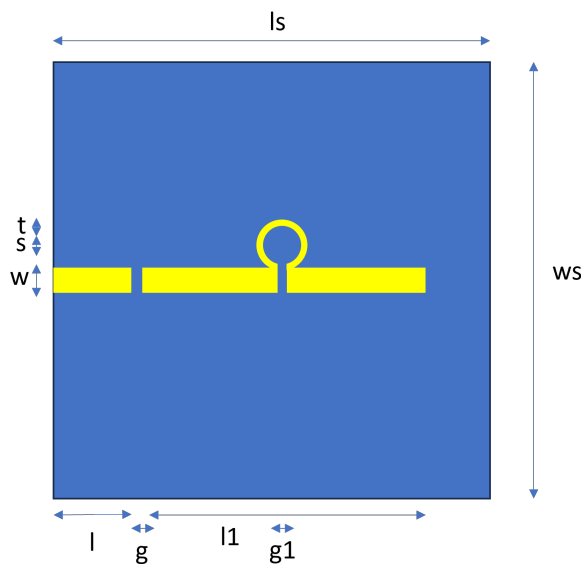


Figure 6: Top view of Omega Resonator

### 3.2.2 Simulation

Using CST Microwave Studio, we created this envisioned geometry. The material we will use to fabricate this material is AD1000 (dielectric) substrate, from Rogers Corporation. It has thickness of 1.5 mm (hs). Its dielectric constant is 10.7, and its loss tangent is 0.0023 (defined at 10 GHz). The copper layer is present at 0.0175 mm (h) thickness on both sides of the dielectric. These parameters are fixed, and the predefined electrical conductivity of Cu is  $5.96 \times 10^7 \text{ sm}^{-1}$  is given in CST software. Now, we will create a resonator of envisioned geometry, considering that resonant frequency should lie in the S-band and impedance stays around  $50 \Omega$ . The simulated structure is shown in Figure 7. The parameters of this structure are given in Figure 8.

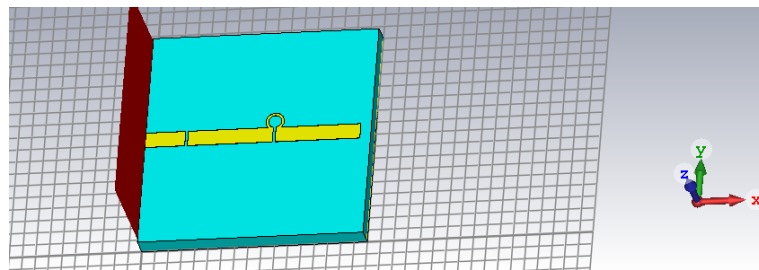


Figure 7: Simulated Omega Resonator

Parameter List					
	Name	Expression	Value	Descrip	Type
-	g	= 0.2	0.2	Undefi▼	
-	g1	= 0.2	0.2	Undefi▼	
-	h	= 0.0175	0.0175	Undefi▼	
-	hs	= 1.5	1.5	Undefi▼	
-	I	= 3	3	Undefi▼	
-	I1	= 13	13	Undefi▼	
-	Is	= 17	17	Undefi▼	
-	s	= 0.5	0.5	Undefi▼	
-	t	= 0.2	0.2	Undefi▼	
-	w	= 1.2	1.2	Undefi▼	
-	ws	= 17	17	Undefi▼	

Figure 8: Parameters of Simulated Omega Resonator

The omega structure's S11 (reflection coefficient) is given in Figure 9. We can see a dip around 3.323 GHz, which is the resonant frequency for our resonator in the ideal case. The magnetic field at the resonant frequency is given in Figure 10. Here, we can see that the magnetic field is highly concentrated at the  $\Omega$  region at the resonant frequency.

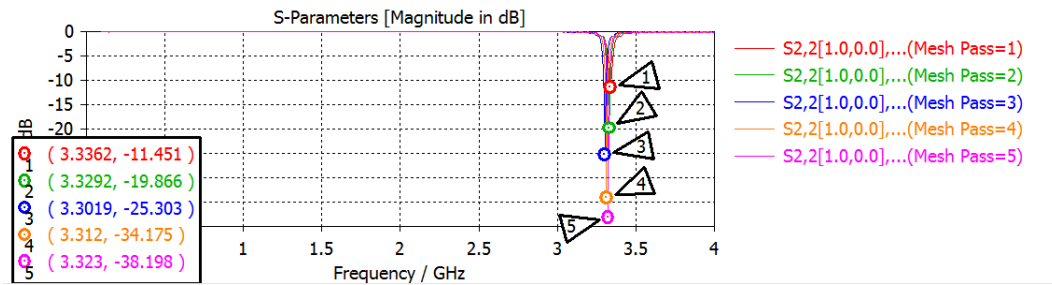


Figure 9: S11 plot from CST Studio

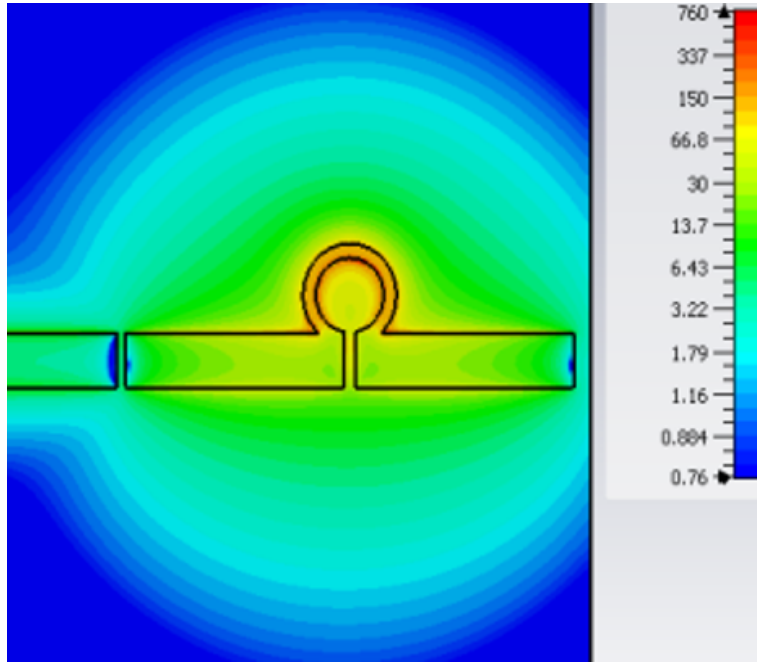


Figure 10: Magnetic Field (simulated) at 3.323 GHz

### 3.2.3 Fabrication Protocol

In this stage, fabrication creates the simulated structure in the real world [8], [10], [3], [9]. This can be explained in the following steps:

1. For substrate, AD1000 (from Rogers Corporation) is selected and cut into  $17 \times 17 \text{ mm}^2$  piece.
2. Rinse the substrate with conc. HCl (35%), isopropanol, acetone, and de-ionized water.
3. For photoresist coating, MICROPOSIT S1813 G2 positive photoresist is used. The spin velocity for this sequence is 4000 rpm for around 1 minute.
4. Prebake this substrate on a hotplate at 110°temperature for around 90 seconds.
5. Using the simulation tools and other software, including CST Studio, AutoCAD, and Foxit Reader, we can create an adequate mask we can use later during UV exposure. This photomask should be printed with a resolution of 1200 DPI.
6. After pasting the mask, the substrate is kept with the photoresist side exposed to UV light (two 9 W bulbs with 365 nm UV radiation from each). It should be exposed for 3 minutes, 15 seconds, in hard contact form.
7. Using MICROPOSIT MF-CD-26, develop the substrate for 60 seconds.
8. Create an etchant solution of 7:2:2 volume of de-ionized water, conc. Hydrochloric acid (35%), and hydrogen peroxide (30%). Etch the substrate for 2 minutes, 30 seconds. Since the lower part of the substrate will act as a ground for our circuit, it must be covered before etching.

9. Using acetone, the photoresist should be stripped. It should be done for 60 seconds.
10. A Subminiature Version A (SMA) connector should be connected to the feedline.

The final omega resonator fabricated is shown in Figure 11.

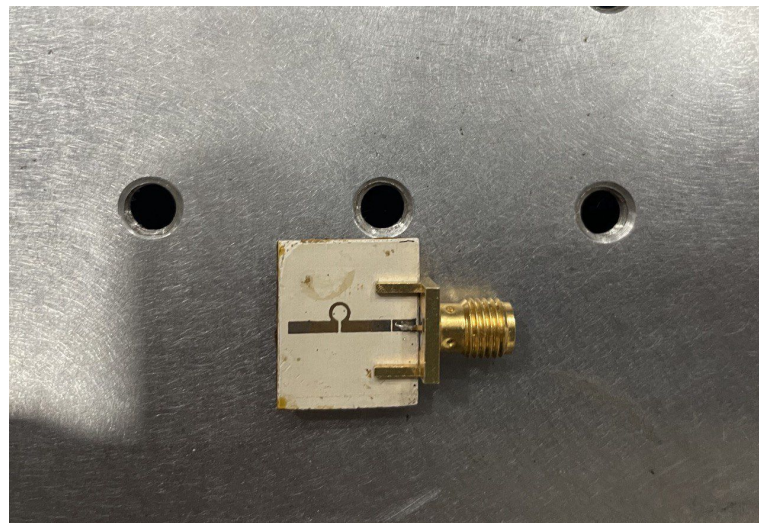


Figure 11: Fabricated Omega Resonator

### 3.3 Superconducting Resonator

#### 3.3.1 Reason for choosing YBCO Superconductor

Yttrium Barium Copper Oxide (YBCO) is a ceramic superconductor with a chemical formula  $YBa_2Cu_3O_7$ . So, it loses all resistance to electric current at lower temperatures. Compared to traditional superconductors, which work at very low temperatures, in order of milli-Kelvin, this superconductor has a very high transition temperature. It can be confirmed from the literature [4] that when the Resistance-Temperature relation was calculated, as shown in Figure 12. According to this literature, the critical temperature was around 90 to 92 K. Still;

there is no exact value since it depends on many factors, including the bulkiness of YBCO. But we can say that compared to traditional superconductors, which work on milli-Kelvin, it is acceptable, as this temperature can easily be reached using a nitrogen bath or Helium compressor.

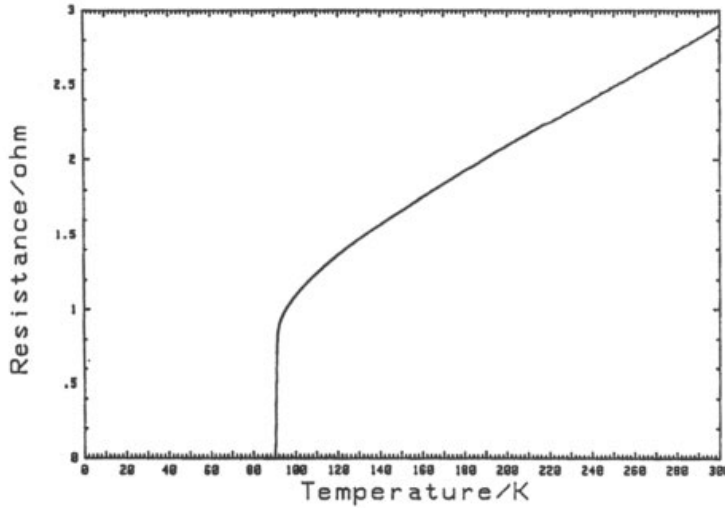


Figure 12: R-T of YBCO from literature [4]

### 3.3.2 Geometry and Simulation

A prototype of a resonator we would like to build has been created, as shown in Figures 13 and 14. This has been developed by considering that resistance ( $Z_{ref}$ ) should be  $50 \Omega$  and resonant frequency lies in S-band. Also, these resonators are two-port resonators, where one will act as input for microwave pulses, and the other will act as output for detecting weak ESR signals.

- Cu as ground and microstrip line (yellow in figure 13)
- AD1000 as a dielectric material used between copper (blue in figure 13)
- LAO, or  $LaAlO_3$ , acts as a substrate in PLD (pink in figure 13)

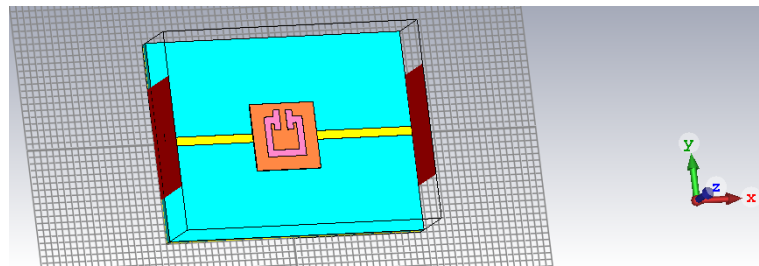


Figure 13: Prototype of YBCO Resonator

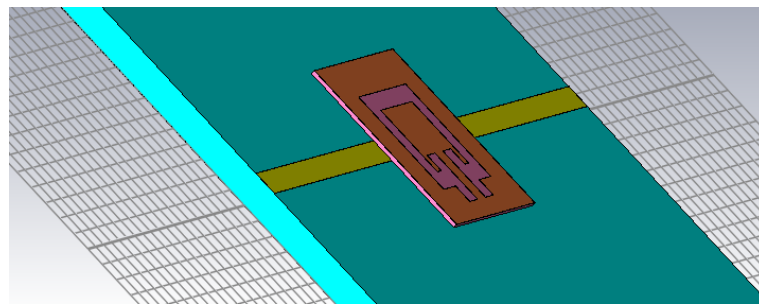


Figure 14: Side view of this simulated resonator

- YBCO, or Y-123, acts as a target in PLD (orange in figure 13) (the gap in YBCO can be fabricated out after deposition using PLD)

The S21 (transmission coefficient), since it's a two-port resonator, for this resonator using simulation is shown in Figure 15. Also, the magnetic field at the resonant frequency is shown in Figure 16. When we calculated the quality factor for the same structure resonator for copper and YBCO, it was found that the YBCO resonator has around 2.88 times higher Q factor than that of Cu.

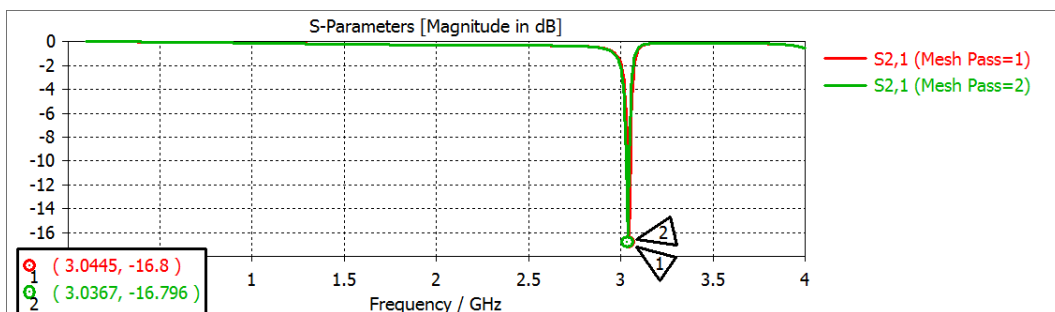


Figure 15: S21 plot from CST Studio

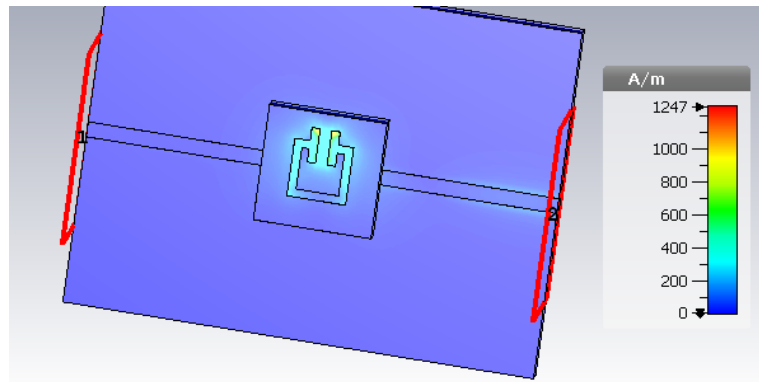


Figure 16: Magnetic Field (simulated) at 3.0367 GHz

### 3.3.3 Creation of YBCO Palette

To make this resonator, we need to create a YBCO palette which can be kept in a pulsed laser deposition chamber. To do so, we need to ensure the powdered material we have is pure. To check that, we will perform X-Ray Detection (XRD) on YBCO before and after the creation of the palette and will compare it with the literature [5] XRD data of YBCO, as shown in Figure 17.

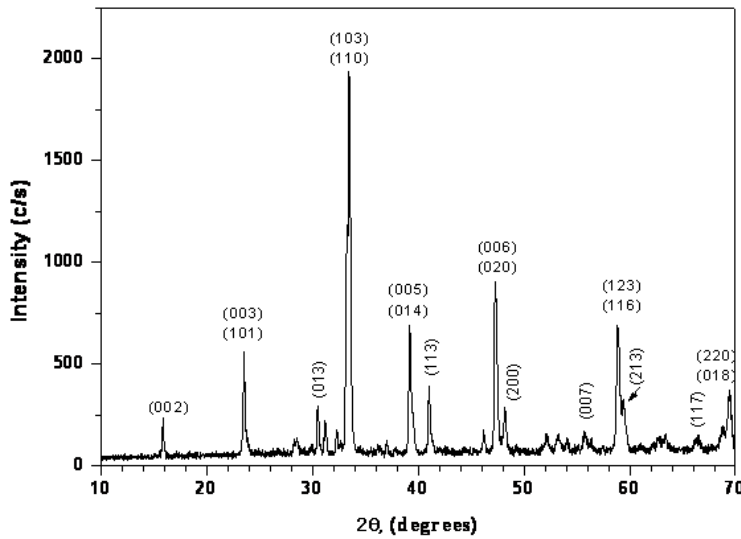


Figure 17: XRD Spectra of YBCO from literature e [5]

Before starting the process of palette creation, we checked the XRD of the

available powder sample. XRD Spectra of YBCO powder are given in Figure 18 before creating the palette.

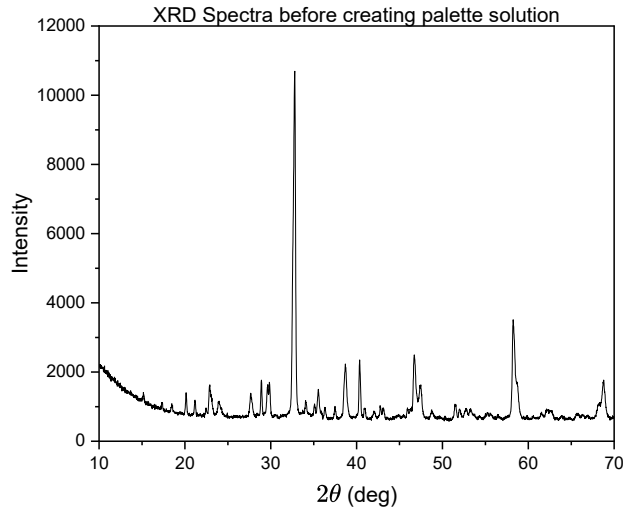


Figure 18: XRD Spectra of YBCO powder

To create a palette, we need a binder solution. Binder solution is made using polyvinyl alcohol (PVA) and de-ionized water in a weight ratio of 1:8. We stirred this mixture at 600 rpm in a magnetic stirrer while increasing the temperature slowly from 333K to 353K. This will take around 1.5 to 2 hours to dissolve in the water completely. Then, this solution is added to YBCO in a weight fraction of 28.5% as suggested in the literature [12] and grind until it becomes a homogeneous paste. Then, 7.5 tons of pressure were applied to this palette to make a coin-size palette. This palette must then be stored in the furnace for around two days. The below order should be applied to the furnace for heating and then cooling:

1. From room temperature to 150°C at the rate of 1°C/min.
2. From 150°C to 180°C at the rate of 0.25°C/min.

3. Stay at 180°C for 1 hr.
4. From 180°C to 950°C at the rate of 2°C/min.
5. Stay at 950°C for 24 hr.
6. From 950°C to 40°C at the rate of 1.5°C/min.

We then performed XRD on this YBCO, shown in Figure 19. After completing the whole process, we can get the YBCO palette. This can be seen in Figure 20—this palette can be used to do R-T and create a resonator using pulsed laser deposition. Further work can be done on this resonator to make it a better resonator.

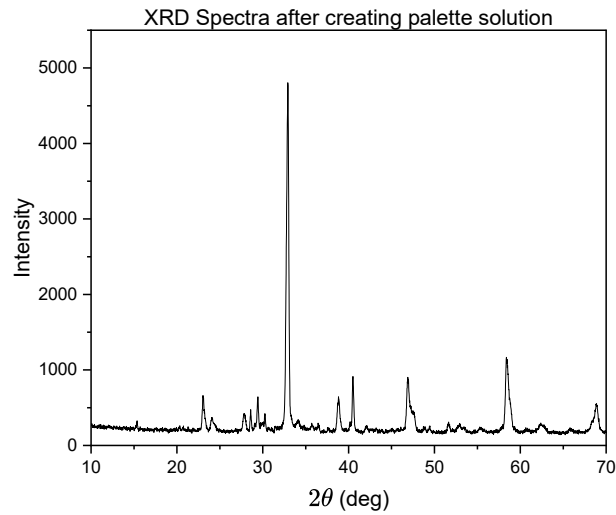


Figure 19: XRD Spectra of YBCO Palette



Figure 20: YBCO Palette

## Chapter 4

# 4 Experimental Instruments

## 4.1 Introduction

The pulsed electron spin resonance spectrometer has the same principle as any transmitter-receiver system in analog communications, as seen in Figure 21.



Figure 21: Transmitter-Receiver System

Transmitter components provide a time-dependent electromagnetic field with high power to the resonator (and finally to the sample), and receiver components take a weak ESR signal from the resonator and then send it to an oscilloscope for detection and analysis. It is generally of the order of mWatt or nWatt. So, we will study the pulsed electron spin resonance circuit in two parts: the transmitter and receiver circuits.

## 4.2 Transmitter Circuit and its components

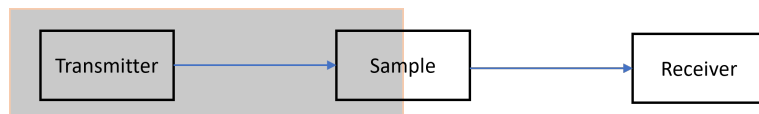


Figure 22: Transmitter System

As discussed above, this part is responsible for providing microwave fields (pulses) with high energy to our sample. This will be used to manipulate our

qubits (applying a single-qubit gate) from their constant alignment with the applied static magnetic field. The circuit diagram for the transmitter part can be found in Figure 23.

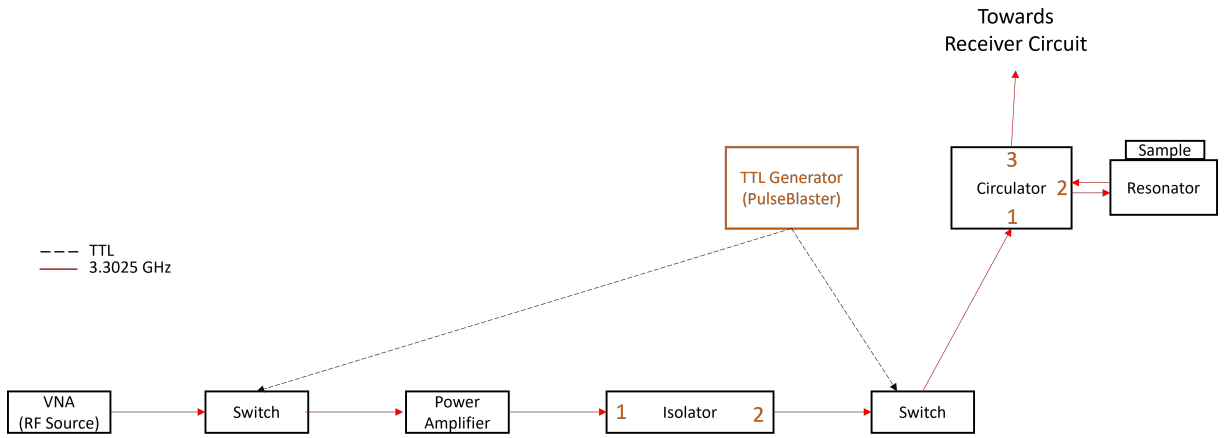


Figure 23: Transmitter Part of Pulsed ESR circuit

We will discuss each component one by one in this session.

### 4.2.1 RF Source (Vector Network Analyzer)

The vector network analyzer (VNA) acts as a high-power source of microwave pulses for our sample. The model we are using for VNA is the Rhode & Schwartz ZVA24, which has two ports, as shown in Figure 24. Each of these ports is capable of generating and detecting microwave pulses. So, we can use this device to generate microwave pulses continuously. We also used this device to check every point of the circuit by exploiting its two ports. So we might not damage some of the sensitive instruments that we are using in our pulsed electron spin resonance experiment. Once the circuit is complete and all devices are in place after double-checking using VNA, we will fix an output frequency that is equivalent to our resonance frequency and lies in the S-band. As we will see later, this frequency also changes with temperature, so we need to keep changing

this output frequency either manually or automatically using code. We will also keep power according to our sample and circuit to make sure we don't damage any sensitive devices in the process. Generally, we can fix this issue using an attenuator, as we will see in later subsections.



Figure 24: Vector Network Analyzer

The Noise Floor of this vector network analyzer is around -98 dBm (as can be seen in Figure 25), so we should always try to keep our signal above this noise floor.

#### 4.2.2 Switch (first)

As discussed in the previous subsection, VNA is responsible for providing microwave pulses, but it is not capable of delivering pulsed microwaves but continuous microwaves. So, in order to do pulsed electron spin resonance, we need to convert these continuous microwaves to pulsed microwaves, which can be done by the first switch. The model we are using for VNA is the Mini-Circuits ZASWA2-50DR-FA+, which is connected to bias (5V), TTL (PulseBlaster), and RF input, as shown in Figure 26.

The TTL (transistor-transistor-logic) source used for this and other switches in our pulsed ESR circuit is PulseBlaster, particularly model PBESR-PRO-300-

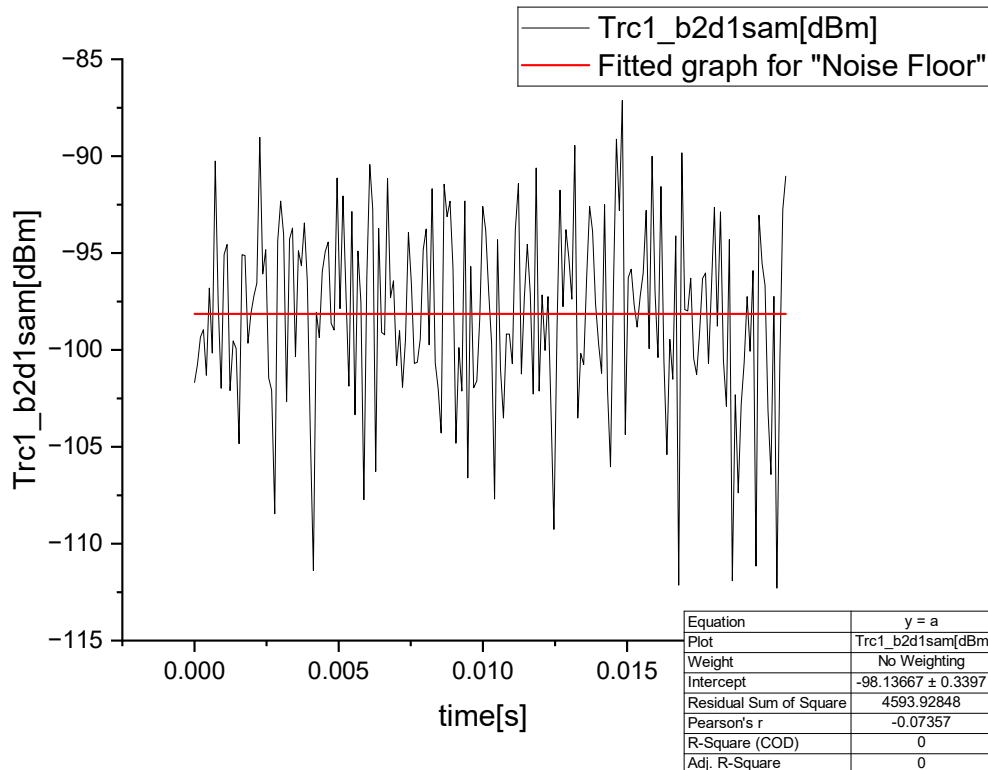


Figure 25: Noise Floor of Vector Network Analyzer



Figure 26: Switch

USB-RM from SpinCore Technologies, Inc. (Figure 27). Its task is to provide a square waveform (square pulsed wave) of a time period according to our requirements. This time period will be of the order of a nanosecond. We can provide these values to the pulseblaster using a computer.



Figure 27: PulseBlaster

Once everything is set in motion, i.e., a 5-volt bias DC voltage is provided, the desired TTL signal (square waveform, for example, as shown in Figure 28) is provided. A microwave is provided on the input using VNA; it can get a pulsed microwave output as we require for a pulsed ESR experiment. When the TTL signal of  $10 \mu s$  is applied, the final output RF after providing input of continuous microwave pulses from VNA can seen in Figure 29

#### 4.2.3 Power Amplifier

We get a pulsed microwave after passing through the switch, but the pulse length is inversely proportional to the applied magnetic field. So, in order to get a  $\frac{\pi}{2}$  pulse when a low magnetic field is used, the time required will be much greater than the relaxation time of FID signals. So, because of this reason, one may not even get the desired FID signals. For this reason, we amplify the magnetic part of the microwave signal using a power amplifier. The model of our amplifier is ZHL-42+, which can be seen in Figure 30.

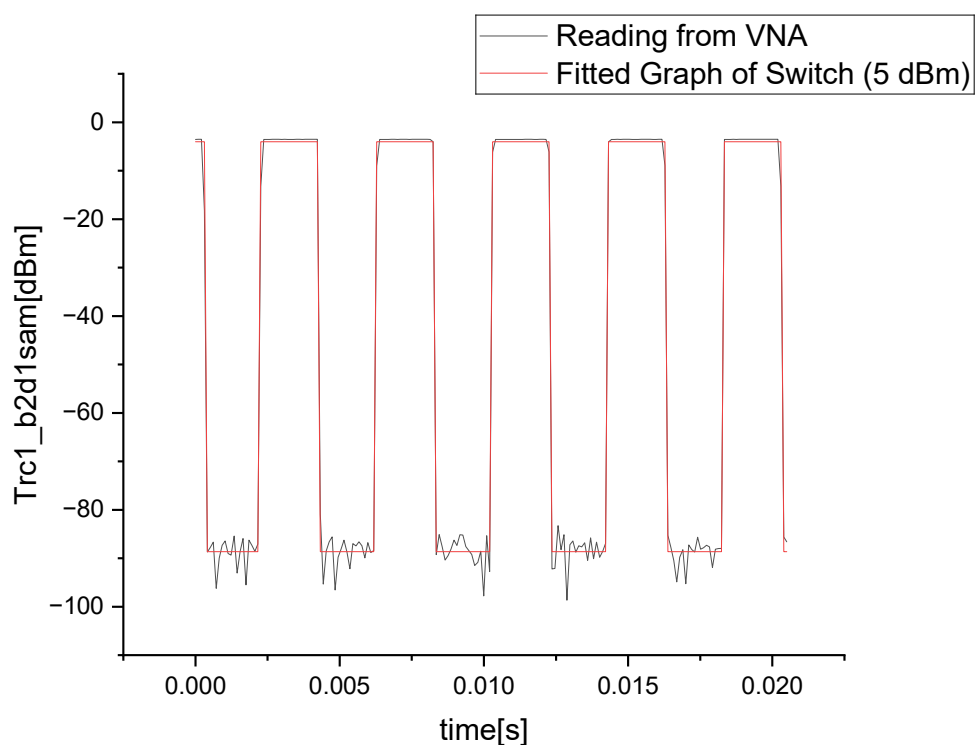


Figure 28: TTL applied on switch

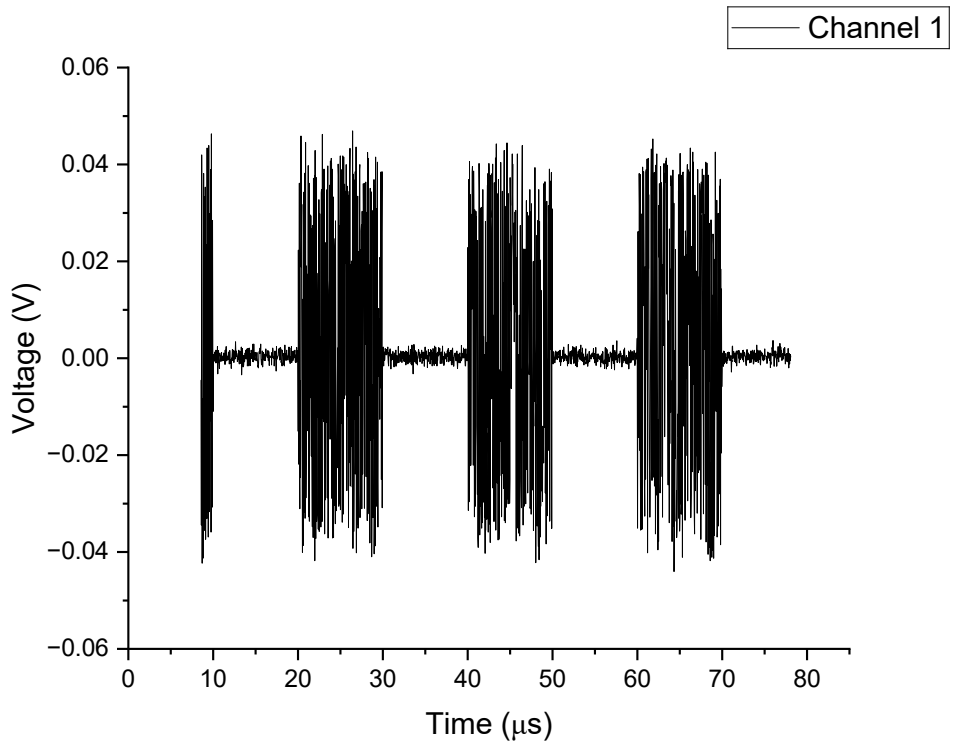


Figure 29: Output RF after passing through switch

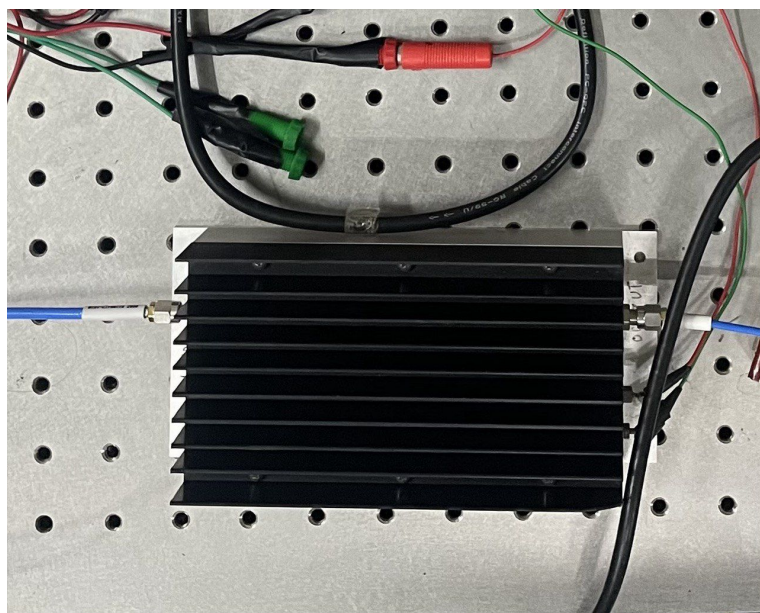


Figure 30: Power Amplifier

#### 4.2.4 Isolator

The isolator is used as a precautionary device to protect devices from any reflection from microwave pulses. It is a two-port device that only works in unidirection, i.e., it allows transmission of microwave power from input (1st port) to output (2nd port) but allows no reflection back towards the input since it attenuates any microwave reflection from the circuit. So it protects the power amplifier from any damage. The model of isolator we are using is Wenteq Microwave F2112-0300-67, as shown in Figure 31

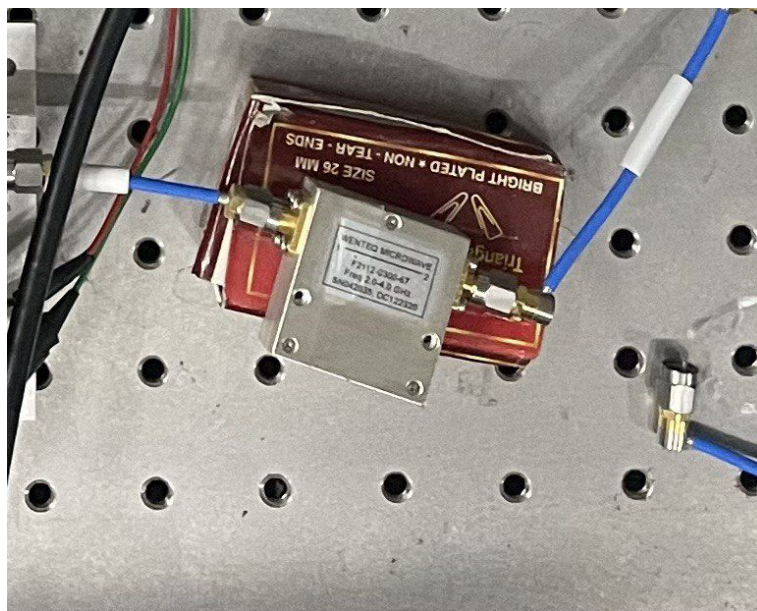


Figure 31: Isolator

#### 4.2.5 Switch (second)

The mechanics of the switch are the same as mentioned in the previous switch section. We will take another input from TTL (PulseBlaster), although the TTL square waveform input will be identical to that of the first switch. The main purpose of using this second switch is to nullify the power amplifier effect cre-

ated during the off period. The power amplifier not only amplifies the pulsed microwave signal during the on period but also amplifies the off signal to some extent. So, to nullify this effect before reaching the sample to stop any unnecessary noise in our final ESR signal, which is already weak to detect, we applied this switch to blank the power amplifier.

### 4.3 Central parts of the circuit



Figure 32: Central part of the circuit

The central part of our circuit consists of a circulator, a resonator, a sample, an electromagnet, and a cryostat. In this session, we will discuss each component of this part of the pulsed ESR circuit. This part is responsible for providing the processed microwave pulses to the sample through a resonator, detecting the weak ESR signal, and sending them to the receiver circuit, which we will discuss later. Also, in this session, we will discuss the electromagnet used to provide a constant magnetic field to our resonator and sample, which is not illustrated in the circuit diagram. The circuit diagram for this part can be found in Figure 33

#### 4.3.1 Circulator

The circulator has the same principle as the isolator, i.e., uni-directional, but there is a little difference since it is three-port rather than two-port like the isolator. It follows an orientation in which microwave pulses circulate from one port to another, i.e., allowing passage from port 1 to port 2, not vice versa and

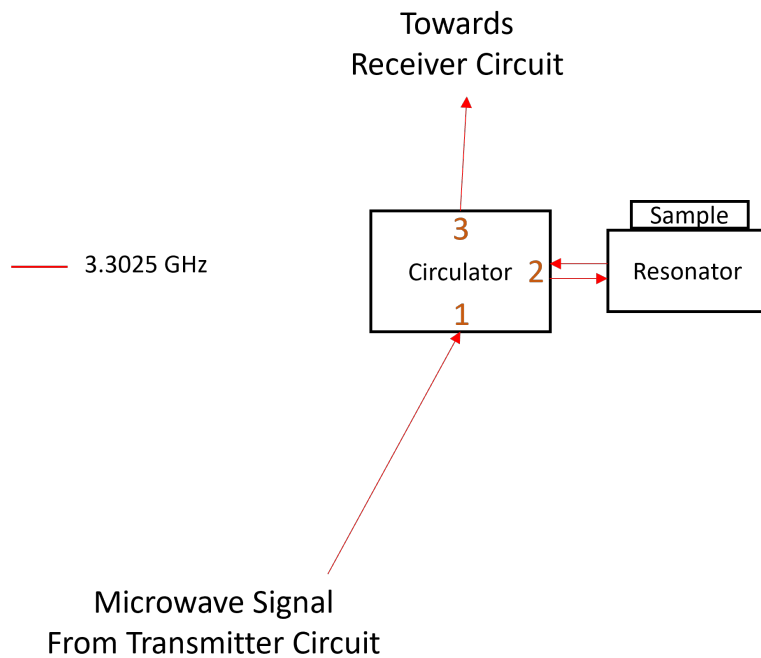


Figure 33: Central circuit

from port 2 to port 3, not vice versa. All other possible routes are blocked for the transmission of microwave pulses. The circulator model used in our experimentation is the Wenteq microwave F2622-0300-67S, as shown in Figure 34. As seen before, the resonator is responsible for providing a microwave signal to the resonator received from the transmitter circuit, detecting weak ESR signals from the sample, and sending them to the receiver circuit. So, we need a device connected to the resonator and sample with different inputs and outputs that can be attached to the transmitter and receiver circuits, respectively. Here, the circulator comes into the picture. We can attach a transmitter circuit at port 1, a resonator at port 2, and a receiver circuit at port 3. So, microwave signals are transmitted from port 1 to port 2 to the resonator. When detecting weak ESR signals, the resonator will send them to port 2, which will then be forwarded to port 3 and finally to the receiver circuit.



Figure 34: Circulator

#### 4.3.2 Resonator

The resonator is required to provide a microwave field to our sample and detect weak ESR signals. We are using a planar resonator for this purpose. This resonator should have a fixed resonant frequency at a given temperature. We will use an omega resonator (as shown in Figure 35) for ESR experimentation, which was discussed in depth in the previous chapter.



Figure 35: Omega Resonator

### 4.3.3 Electromagnet and Cryostat



Figure 36: Electromagnet and Cryostat

The electromagnet provides a static magnetic field for the sample, creating a two-level system for our experimentation. Figure 36 shows electromagnet and cryostat. This electromagnet's power supply (Figure 37) can be controlled using a computer, enabling us to work remotely.

We will be working on different temperatures, not only at room temperature, so we will be using cryostat for that purpose. In an ideal situation, it should go to 4K using Helium. Still, we won't use a radiation shield (Figure 38) due to



Figure 37: Power supply of Electromagnet

issues arriving while connecting inside the cryostat between the resonator and ESR circuit. We were still able to reach a temperature of 8K. So, we decided to calculate values up to 10K for better accuracy.



Figure 38: Radiation shield

It is a single-chamber cryostat. So, after making the required connection and closing the cryostat chamber, we need to create a vacuum. We first turned on the rotary to achieve this goal until the pressure inside the chamber reached below 4.6E+0 mbar. Then, we started the vacuum pump motor, which went

to a frequency of 1500 Hz. Once we reached pressure below 4.0E-4 mbar, we were good to start cryostat. We then started chilling and waited till it reached a temperature between 291K and 295K. Then, we started the compressor, which decreased the temperature inside the chamber. We controlled the temperature inside the chamber using its instrumentation. This is a general mechanism for utilizing the cryostat.

#### 4.3.4 Sample

For pulsed electron spin resonance, we need materials that are paramagnetic in nature or free radicals. The most commonly used samples for exploitation in electron spin resonance experiments are Galvinoxyl and DPPH (2,2-diphenyl-1-picrylhydrazyl). We will be working with DPPH in our experimentation. DPPH has a very short coherence time. We kept this sample in the loop of that resonator, where the magnetic field was highest during resonant frequency. Rather than placing the sample powder directly on the surface of the planar resonator, we will cover it up with Teflon tape and stick it to the resonator so that it won't get removed by the vacuum pump in the cryostat chamber.

### 4.4 Receiver Circuit and its components

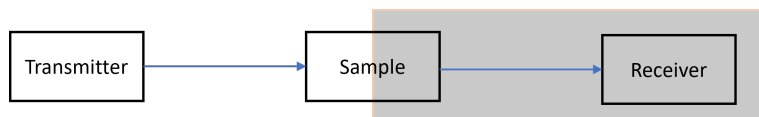


Figure 39: Receiver System

This part is responsible for detecting weak ESR signals. The signal coming from the circulator is 3.3025 GHz, which an oscilloscope cannot detect. So, in this circuit, we will decrease the bandwidth to below 500 MHz, which can be

detected from the oscilloscope. The circuit diagram for the receiver part can be found in Figure 40. This circuit detects the homodyne signal rather than the traditional heterodyne signal and then envelopes it for further calculation.

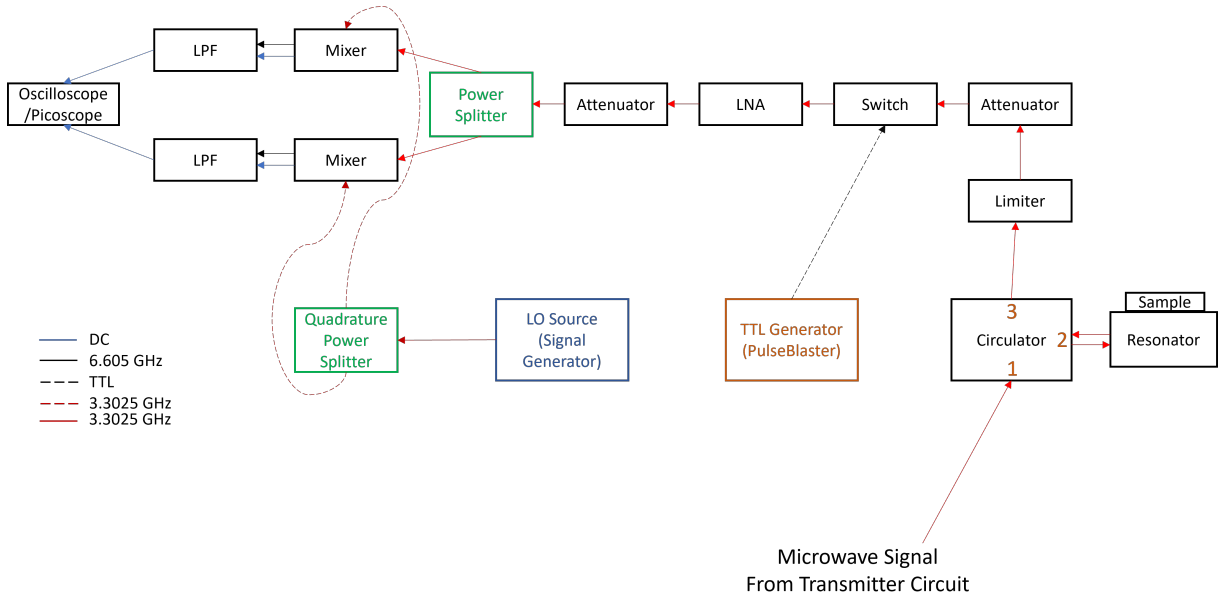


Figure 40: Receiver Part of Pulsed ESR circuit (Homodyne)

We will discuss each component one by one in this session.

#### 4.4.1 Limiter

The limiter is another mini-component of the system which protects the valuable devices used in the receiver part. It limits the flow of power if, in some cases, the ringdown is of high power. It is also important to remember that it is a one-way circuit, so it should always be connected in a specific order. In our case, the limiter model is Mini-Circuits VLM-063-2W-S+, which needs to be connected to the input at the female SMA connector and output at the male SMA connector. This can be seen in Figure 41.



Figure 41: Limiter

#### 4.4.2 Attenuator

The attenuator is used to decrease the power of signals. There are many types of attenuators, like 3 dB attenuators, 6 dB attenuators, 10 dB attenuators, etc. We will be using them according to the requirements at different temperatures. The first attenuator shown in Figure 40 is a 3 dB attenuator, while the other one varies according to our need to get enough data to detect weak ESR signals. Some of the attenuators used are shown in Figure 42. These devices do not generally affect FID signals since they are very weak (around 60 dBm).

#### 4.4.3 Switch (third)

This switch is used to turn off the receiver circuit during the dead time. Generally, the dead time of ESR circuit is 120–130 ns. So, we need to keep the receiver circuit off until the end of the excitation pulse. We can create a proper sequence in PulseBlaster (TTL Source) that needs to be followed, as shown in Figure 43 (time displayed is just for reference, not actual data from the experiment, since we need to keep changing these values).



Figure 42: Attenuators

#### 4.4.4 Low Noise Amplifiers and Attenuators

The FID signals are very weak for pulsed electron spin resonance, so we need to amplify them to be able to detect them for proper measurement. For this purpose, low-noise amplifiers, also known as LNAs, are required to enhance the receiving signals. We must use the appropriate combination of attenuators and LNAs to get desired signals. In our experimentation, we are taking two LNAs and different attenuators depending on the temperature and other conditions we are measuring. One can also use a video amplifier after the mixer and a low-pass filter, but in homodyne, we need two of those, so we choose to use two LNAs instead of one LNA and two video amplifiers. The models of LNAs we used are Wenteq Microwave ABL0400-50-4307 (required 12 volts current) and Mini-Circuits ZX60-63GLN+ (required 5 volts current), as shown in Figure 44.

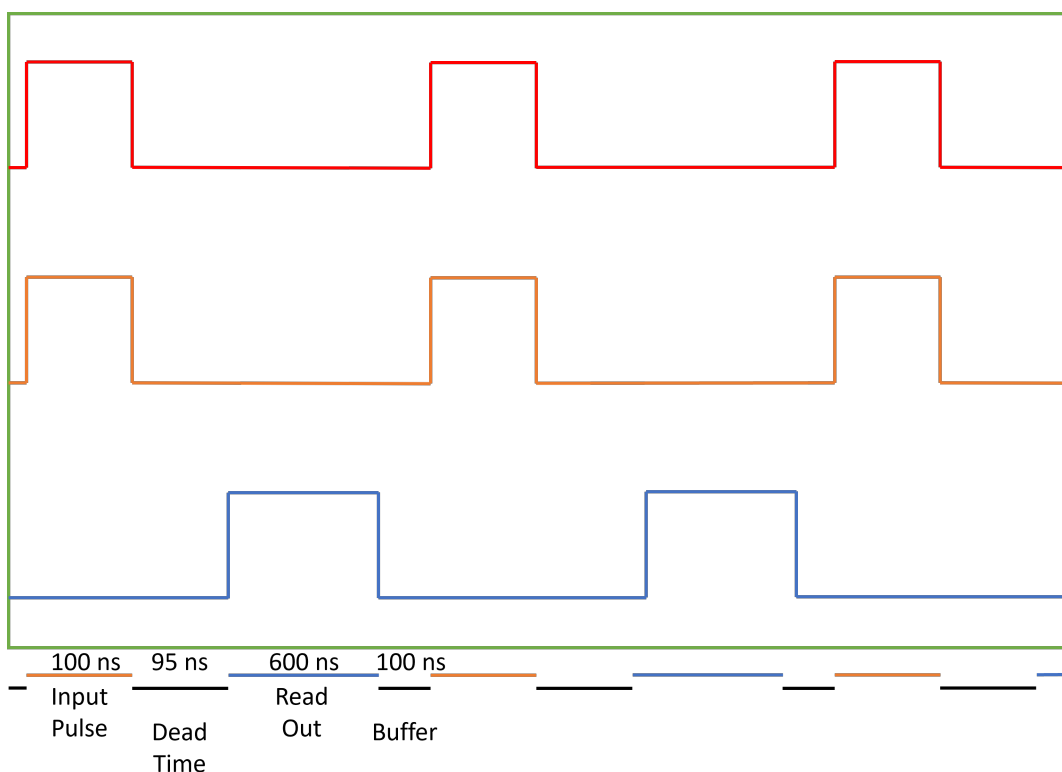


Figure 43: TTL Pulse sequences for different switches



Figure 44: Low Noise Amplifiers

#### 4.4.5 Power Splitter

The power splitter is a passive device known as a  $0^\circ$  splitter. It accepts an input signal from one end and gives multiple outputs on the other. This output signal has specific phase and amplitude characteristics. A  $0^\circ$  splitter provides equal amplitude and a  $0^\circ$  phase relation between output signals (as shown in Figure 45). Each of these output signals also has high isolation.



Figure 45: Characteristics of Power Splitter

These power splitters have an insertion loss associated with them; the higher

the number of outputs, the greater it is. These can be seen in table 1. This table only shows theoretical values, which are always slightly higher than these. We are using a power splitter with two ports, so the insertion loss is approximately 3 dB, and if we consider a 1 dB loss from connections and other miscellaneous parts, then we must give 4 dB more than what we need in output. For example, if we need 10 dB on the output ports, we should give 14 dB on the input port.

Table 1: Insertion Loss for different number of output ports

Output Ports Count	Insertion Loss (dB)
2	3
3	4.8
4	6
5	7
6	7.8
8	9
10	10
12	10.8
16	12
24	13.8
48	16.8

These devices can also be used as power combiners when in opposite configurations. It will take multiple inputs, and depending on their amplitude and phase relations, it will give suitable output on the opposite port. Insertion losses, in this case, differ depending on the properties of the input signals. The model we use for the power splitter is Mini-Circuits ZAPD-4-S+, as shown in Figure 46.

#### 4.4.6 LO Source (Signal Generator)

This device will act as a local oscillator for the mixer, which we are going to use in a later circuit. The frequency mixer will require a frequency equivalent to that of input (i.e., in the S-band), so this device requires sending this



Figure 46: Power Splitter

necessary signal for the LO of the mixer. We will discuss further use in a later session. The signal generation model we are using is Anapico APSIN4010, 9 KHz–4 GHz, as shown in Figure 47.

#### 4.4.7 Quadrature Power Splitter

The working process is almost similar to that of a power splitter. It accepts an input signal from one end and gives multiple outputs on the other. This output signal has specific phase and amplitude characteristics. This splitter provides equal amplitude and a  $90^\circ$ phase relation between output signals (as shown in Figure 48). Each of these output signals also has high isolation. That's why this power splitter is also called a  $90^\circ$ splitter.

We are using a quadrature power splitter with two ports, so the insertion loss is approximately 3 dB, the same as that of a power splitter. Considering 1 dB loss from connections and other miscellaneous parts, we must give 4 dB more



Figure 47: Signal Generator



Figure 48: Characteristics of Quadrature Power Splitter

than we need in output. The splitter takes input from the signal generator and then sends the outputs to the frequency mixers. These mixers need 10 dB on the LO port, so we should give 14 dB on the input port. The model we use for the quadrature power splitter is Mini-Circuits ZAPDQ-4-S+, as shown in Figure 49.



Figure 49: Quadrature Power Splitter

#### 4.4.8 Frequency Mixer

We are using a power splitter to divide the upcoming signal into two parts, so we need two mixers for this circuit, one for each splitter signal. The signal we have been working on has a frequency of S-band (3–4 GHz), but oscilloscopes and microscopes cannot detect such high frequencies, so we need to lower the frequency. In the case of heterodyne experimentation, it should be less than 500 MHz since we are doing homodyne, so we need to eliminate the frequency. We can do so by applying the same frequency on LO as we are getting from the vector network analyzer. This can be done by the signal generator and quadrature power splitter, as discussed in previous subsections. This will give output with double frequency and DC signal, as shown in Figure 50.

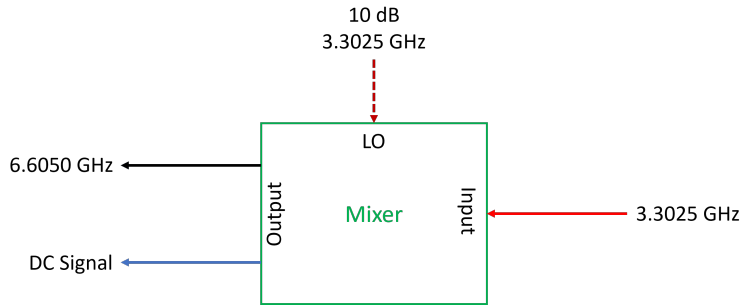


Figure 50: Principle of Frequency Mixer

The power splitter provides two outputs with a  $0^\circ$  phase difference. For example, if the input is  $A\cos(\omega t)$ , then both outputs will be in the same phase, i.e.,  $\frac{A}{2}\cos(\omega t)$ . In case of quadrature power splitter, it gives  $90^\circ$  phase difference, like when input is  $A\cos(\omega t + \phi)$ , outputs are  $\frac{A}{2}\cos(\omega t + \phi)$  and  $\frac{A}{2}\sin(\omega t + \phi)$ . So when we use mixers on these outputs, one mixer will mix  $\frac{A}{2}\cos(\omega t)$  and  $\frac{A}{2}\cos(\omega t + \phi)$  which will give cosine component and other mixer will mix  $\frac{A}{2}\cos(\omega t)$  and  $\frac{A}{2}\sin(\omega t + \phi)$  which will give sine components.

The mixer gives both a double frequency and a DC signal as output (as can be calculated in the above cases). In the next part, we discuss eliminating that double frequency and only detecting the DC signal on the oscilloscope. The model of the frequency mixer used is ZX05-43-S+, as shown in Figure 51.

#### 4.4.9 Low Pass Filter (LPF)

The low pass filter is another mini-component which has a cutoff frequency. This device only allows the passage of frequency, which has a lower frequency than the cutoff frequency. So, this will only enable signals in the range of DC signals to reach their cutoff frequency. So, the double frequency part coming from the frequency mixer is eliminated, and only the DC signal part can pass through. In our case, we are using the VLFX-500+ model of LPF (as shown in



Figure 51: Frequency Mixer

Figure 52, so it only allows signal between DC and 500 MHz. So it will only  $\cos\phi$  term and  $\sin\phi$  term through it.



Figure 52: Low Pass Filter

#### 4.4.10 Oscilloscope and Picoscope

This final converted signal is observed in either oscilloscope (Figure 53) or picoscope (Figure 54). One reading contains a sine component, and the other

contains a cosine component. We will square them and add them to get an amplitude square. Then, we will take the square root of the same to get the desired amplitude value (the code to do so is shown in the appendix).



Figure 53: Oscilloscope

## 4.5 Complete Circuit

The complete circuit can be seen in Figure 55. The physical circuit can be seen in Figure 56.



Figure 54: Picoscope

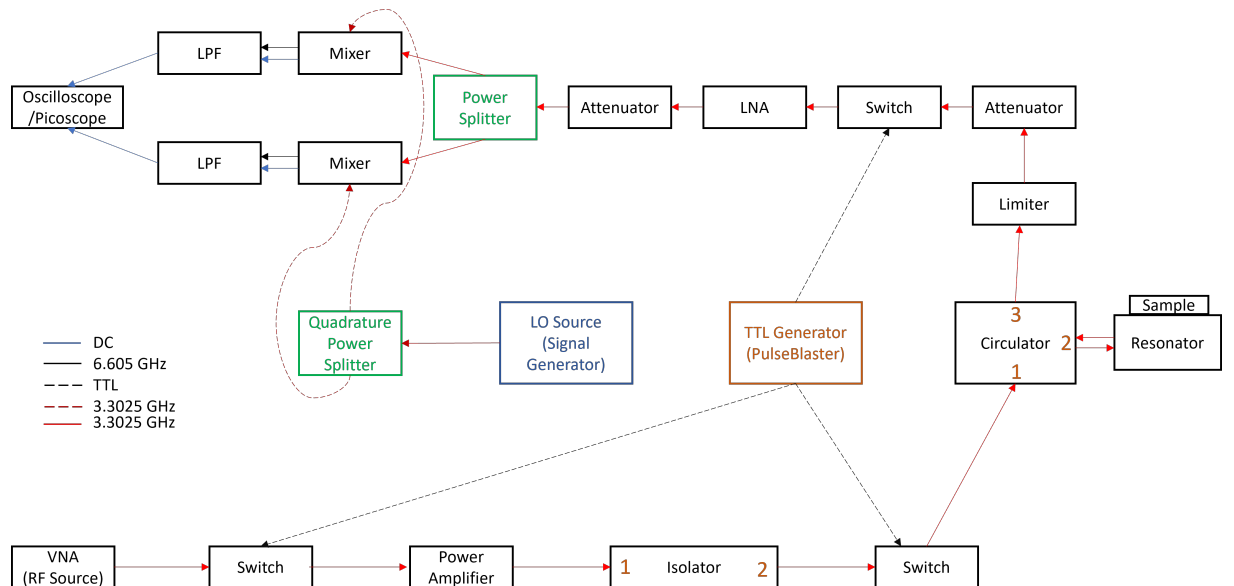


Figure 55: Pulsed ESR Circuit

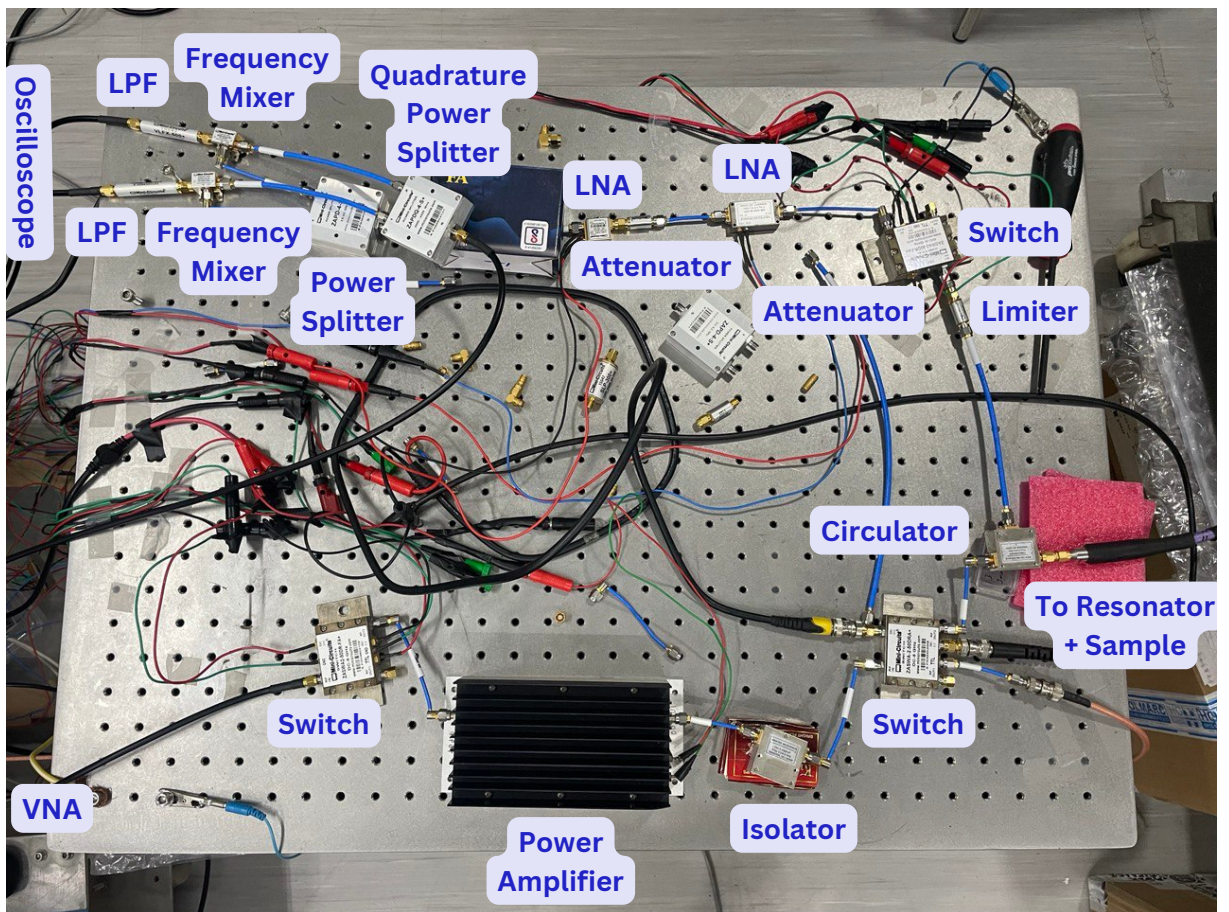


Figure 56: Physical Pulsed ESR Circuit

## Chapter 5

# 5 Data Processing and Results

## 5.1 Omega Resonator and its characteristics

We are going to work with an omega resonator in this whole experiment. When we simulated the omega resonator in CST Microwave Studio, its resonant frequency was 3.323 GHz (as shown in Figure 57), and when we fabricated the resonator, considering the ink spreading of the Canon and doing adequate changes, the resonant frequency with the sample is 3.325 GHz and without a sample is 3.323 GHz, same as simulated one. This data was taken at room temperature.

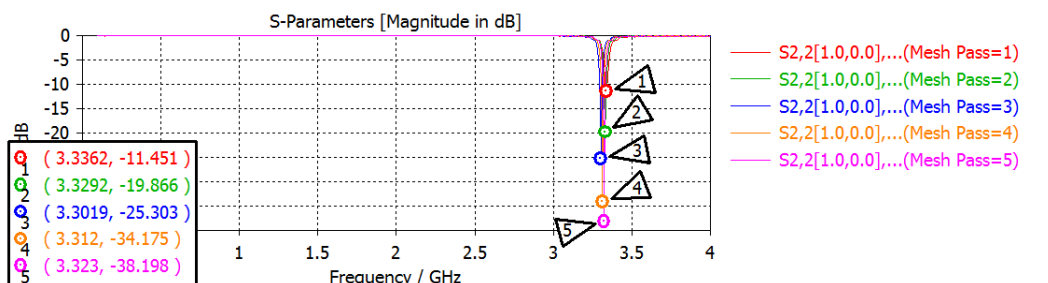


Figure 57: Simulated S11 data of Omega Resonator

We calculated S11 and resonant frequency at many temperatures and tried to get a linear relation between them. But as we proceeded to a low temperature, we encountered another small peak created by the reflection from the connector inside the cryostat due to bending. We tried different connectors, but due to the small size of the cryostat, we could only decrease this small peak so that it wouldn't interfere much with our result. This small peak does not affect our data on room temperature or till 180K (see Figure 58 and Figure 59) temperature,

but after 180K temperature, it passes through our central peak, which creates some distortion in our data (see Figure 60), although it already passes through and doesn't sink with a central peak at lower temperature like 10K temperature (see Figure 61). However, for some reason, it still shows distorted data. We can calculate a relation between temperature and resonant frequency from these variable data points on different temperatures. This relation is shown in Figure 62. As seen in the graph, it distorted the linear path, which affected taking readings below 180K temperature.

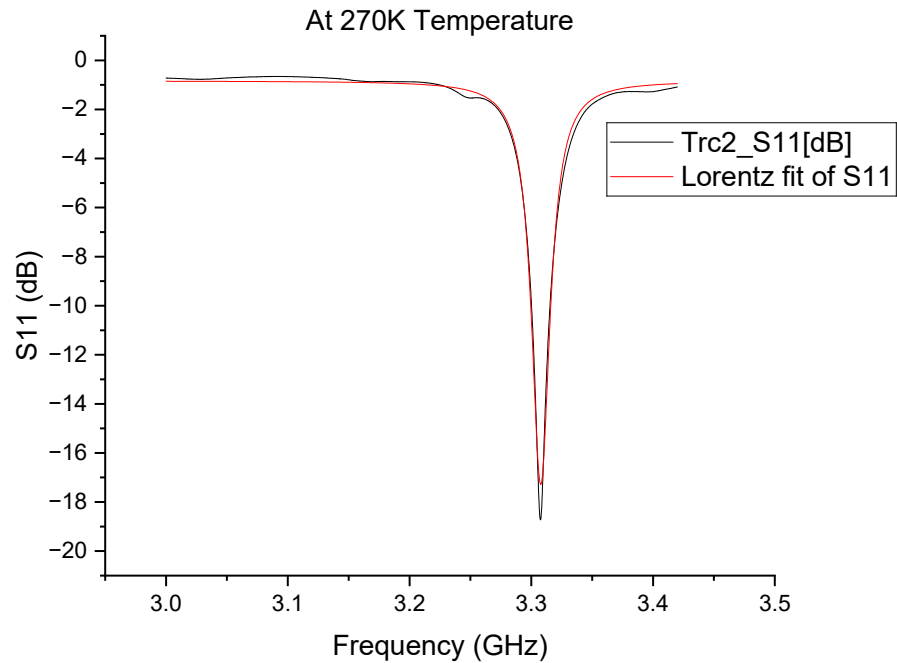


Figure 58: S11 data at 270K Temperature

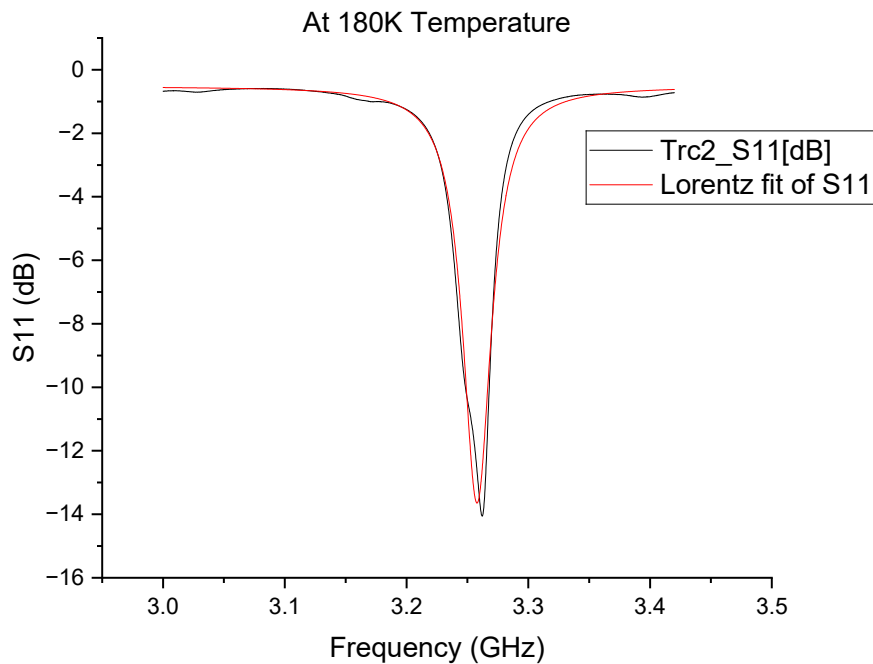


Figure 59: S<sub>11</sub> data at 180K Temperature

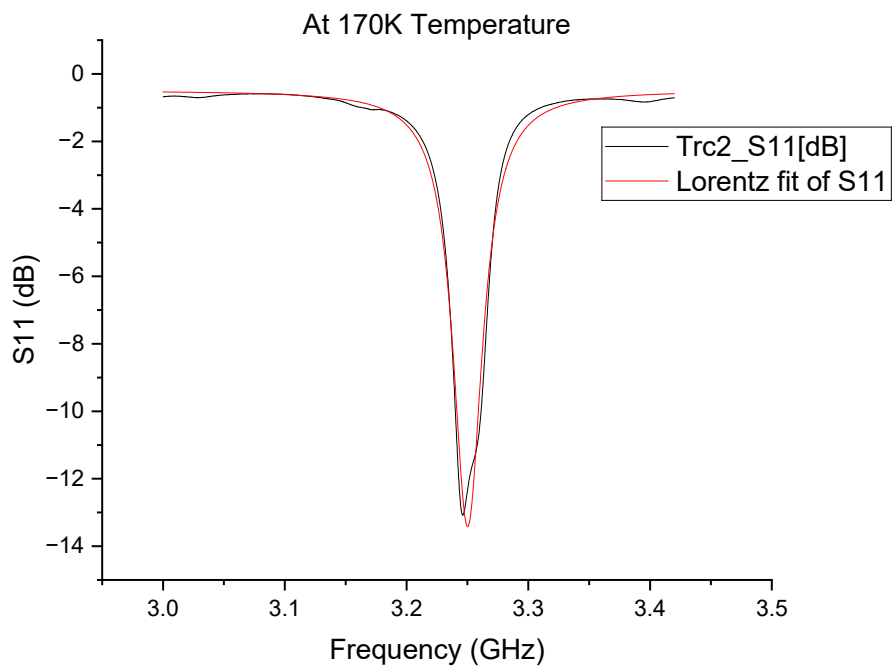


Figure 60: S<sub>11</sub> data at 170K Temperature

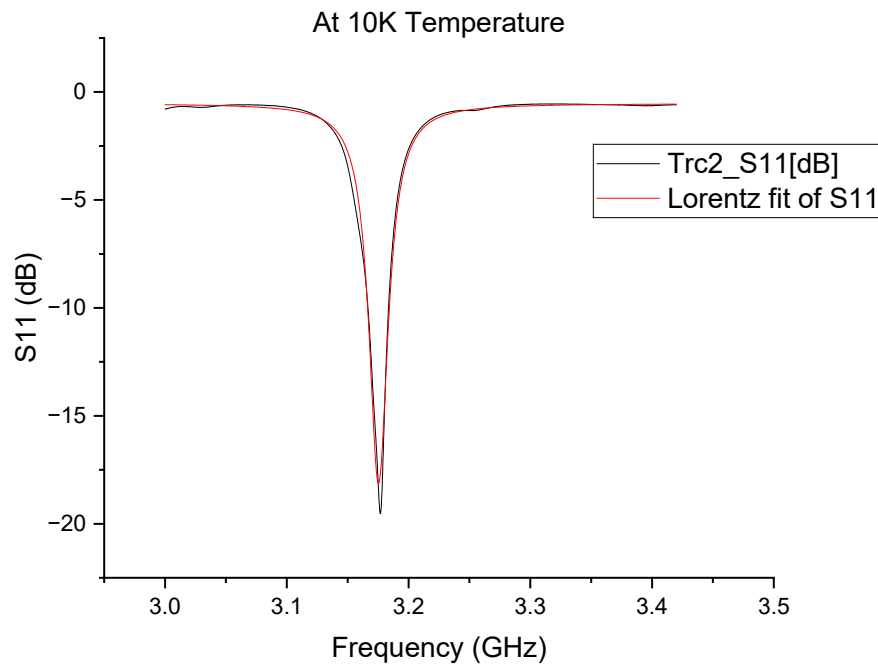


Figure 61: S11 data at 10K Temperature

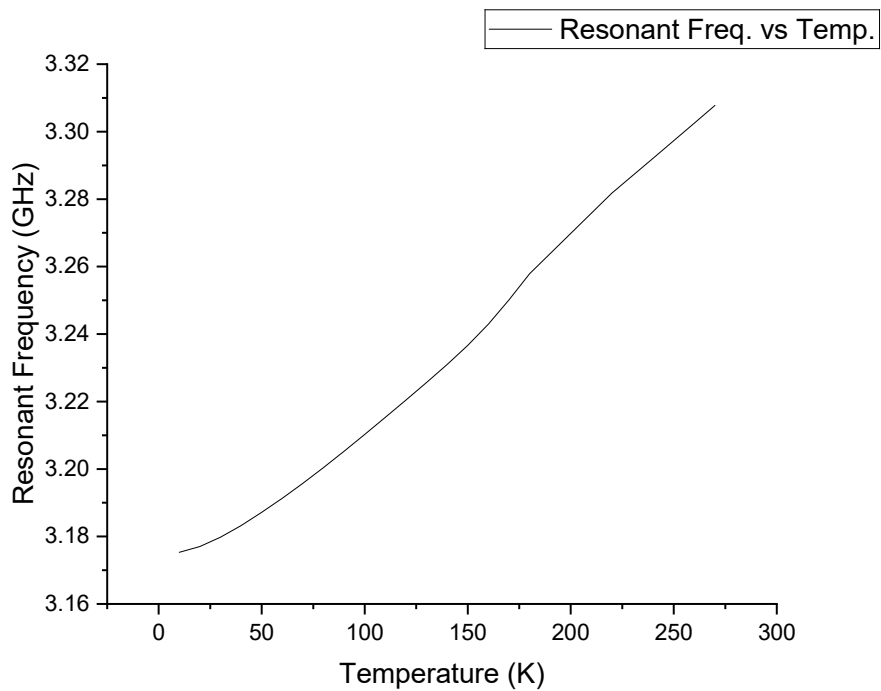


Figure 62: Resonant Frequency vs. Temperature

## 5.2 CW ESR Sprectrum

This spectrum is used to identify the magnetic field at which Zeeman splitting occurs. The same distortion can be seen in this spectrum as in S11 data. The code to perform this experiment is shown in the appendix. To understand it better, we will focus on specific temperatures as we did in the last session and fit them using Lorentz fit, namely, 270K (Figure 63), 180K (Figure 64), 170K (Figure 65), and 10K (Figure 66). These figures show the distortion around 180K and 170K, as in S11. To better understand, we can look at the graph between temperature and electromagnet current (as shown in Figure 67) and also between Resonant frequency and electromagnet current (as shown in Figure 68).

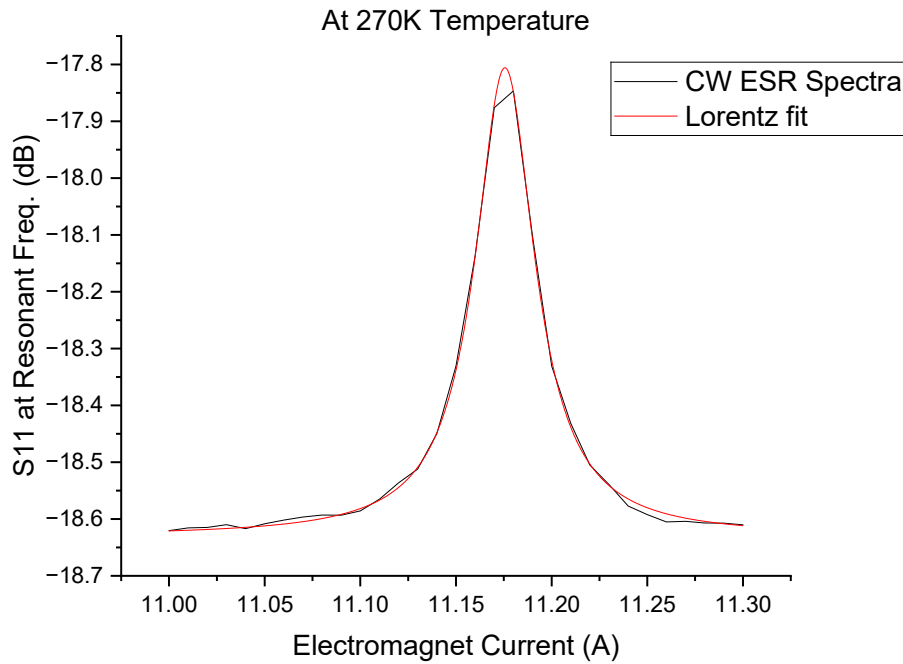


Figure 63: CW ESR spectra at 270K temperature

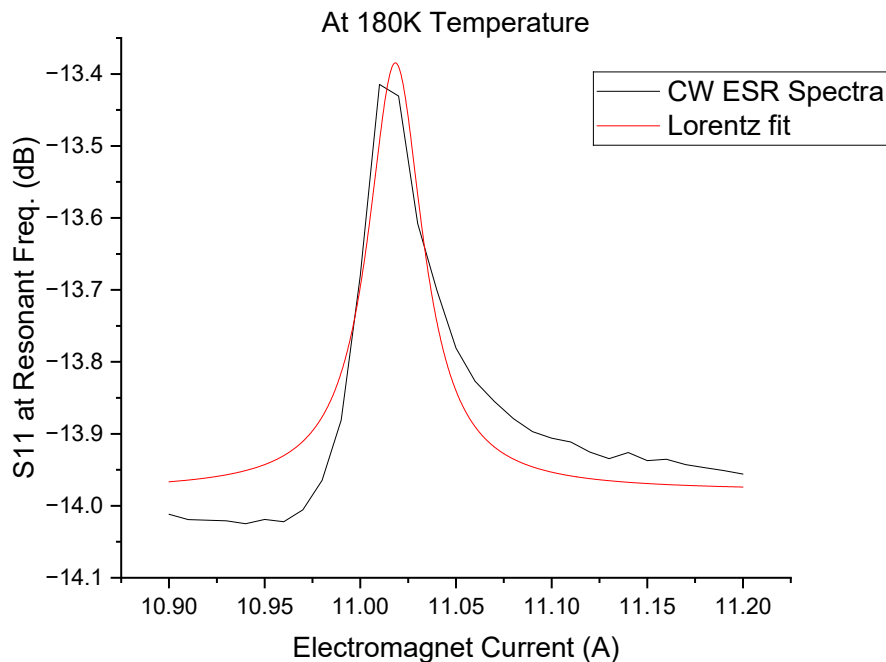


Figure 64: CW ESR spectra at 180K temperature

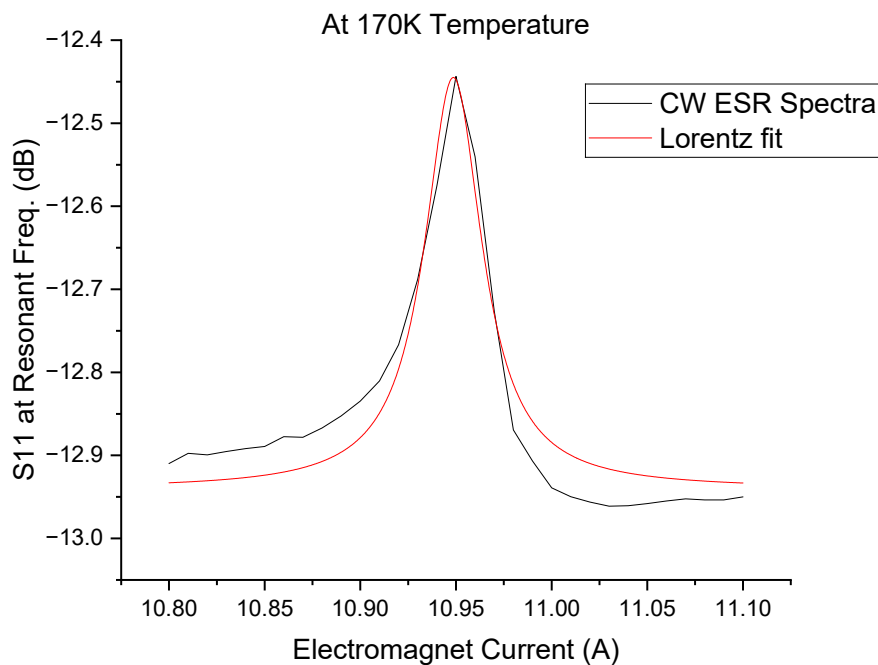


Figure 65: CW ESR spectra at 170K temperature

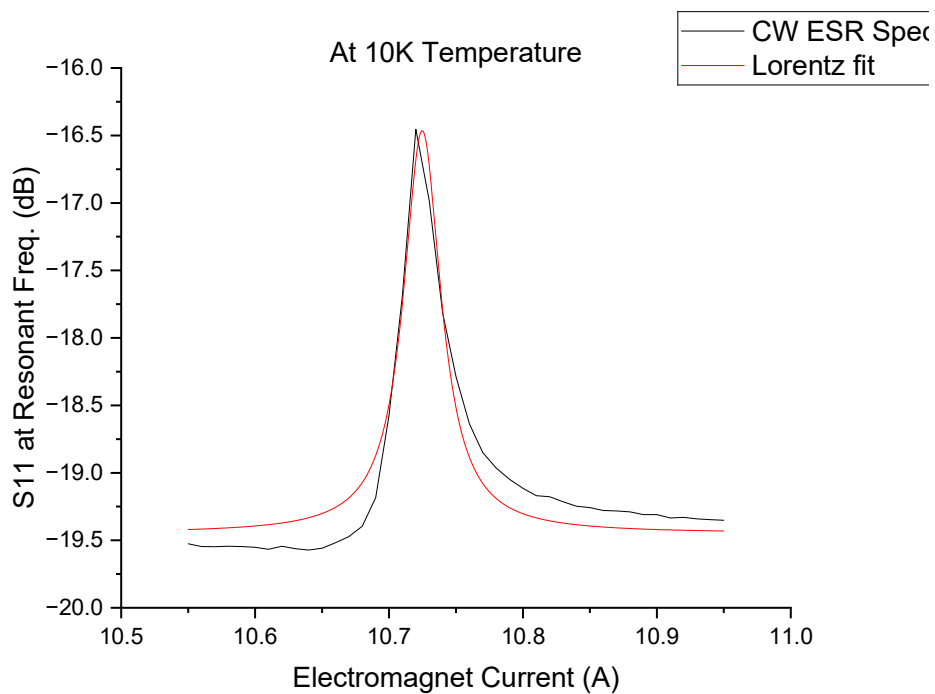


Figure 66: CW ESR spectra at 10K temperature

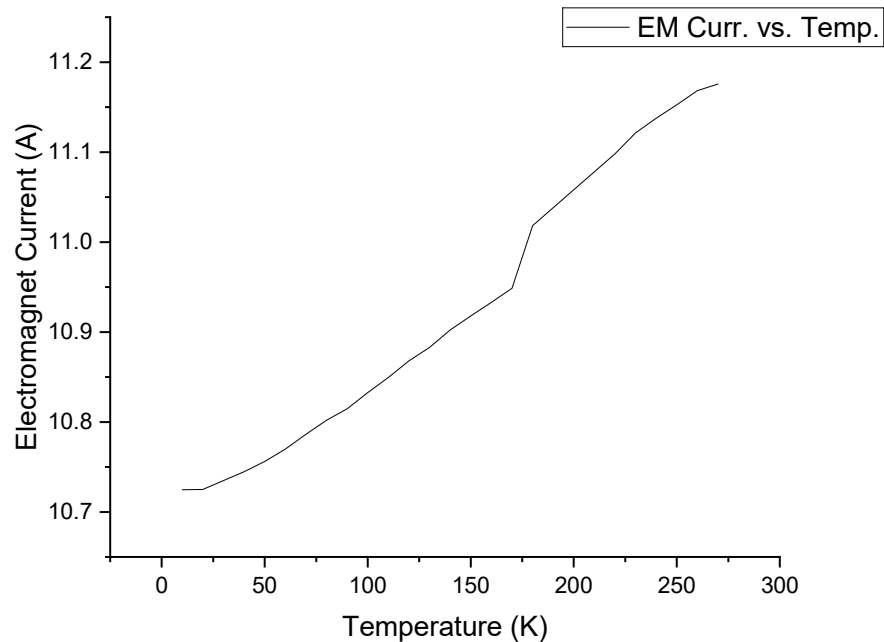


Figure 67: Electromagnet Current vs. Temperature

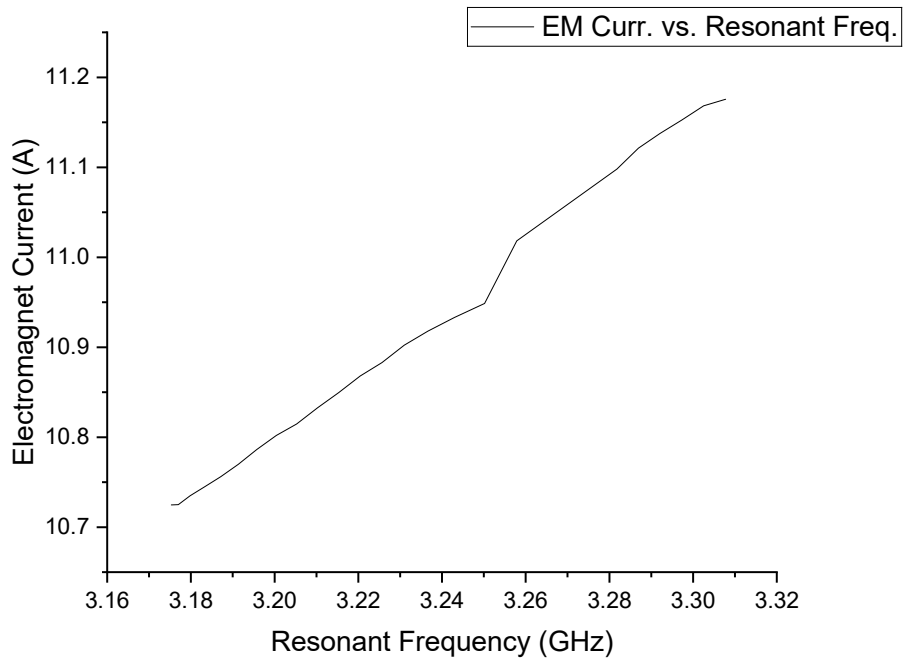


Figure 68: Electromagnet current vs. Resonant Frequency

### 5.3 Pulsed ESR Circuit without Resonator

This is to ensure our circuit works fine before starting homodyne pulsed electron spin resonance. We will run the circuit without connecting to the resonator and sample (i.e., only taking reading for transmitter circuit), but use  $50\Omega$  terminator. This can also help identify how a switch takes to act after TTL as sent in the signal 1 using square waveform. We have used picoscope to calculate the output. This can be seen in Figure 69, and the envelope of the same can be seen in Figure 70.

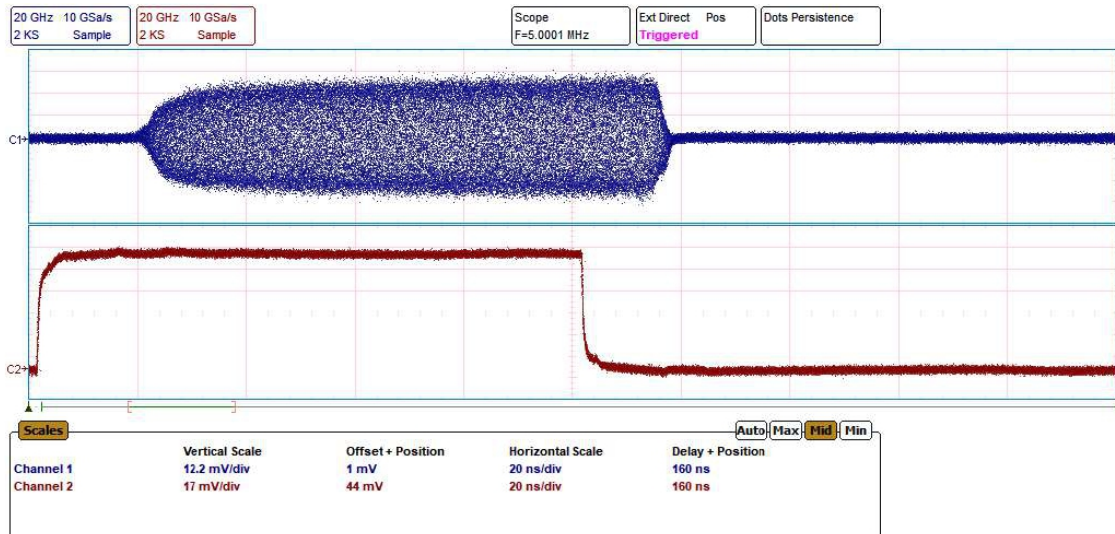


Figure 69: Circuit Output when Resonator+Sample is not connect

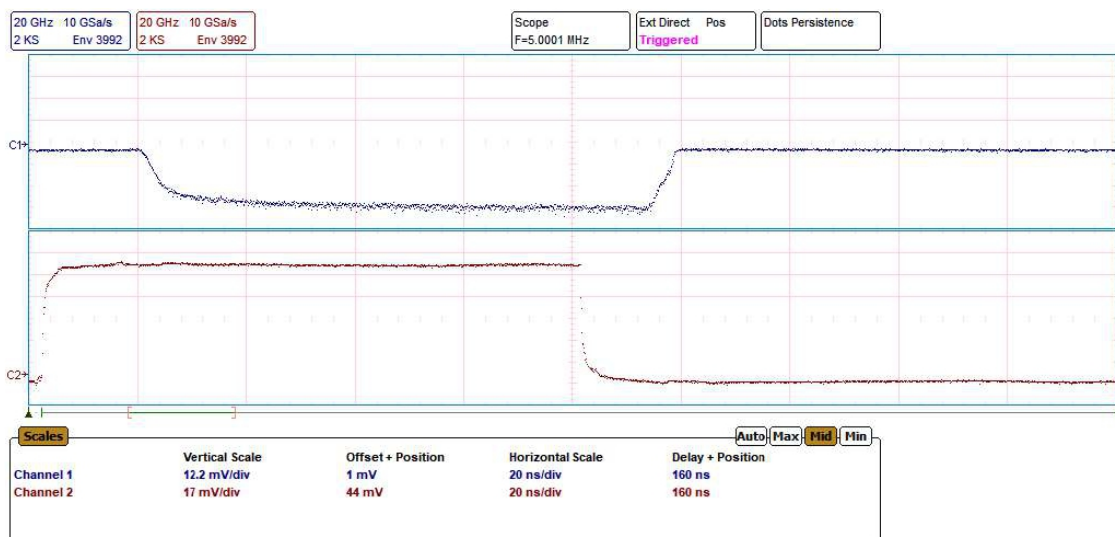


Figure 70: Envelope of the Circuit Output

### 5.4 Ringdown time and Deadtime

Now we will connect the pulsed electron spin resonance circuit with the resonator and sample DP; then we will take the reading from the microscope, which is shown in Figure 71, and the envelope of the same can be seen in Figure 72.

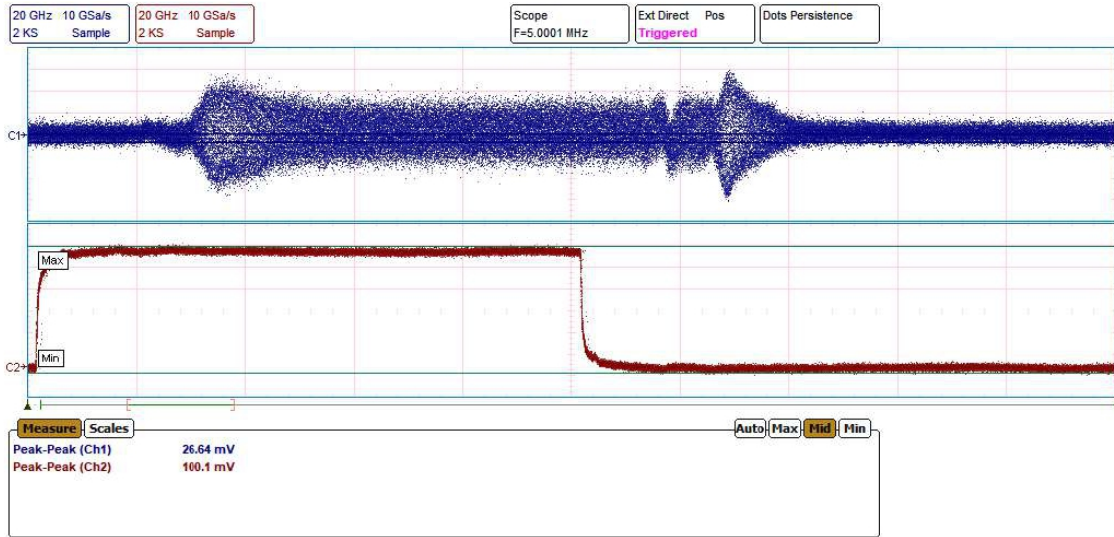


Figure 71: Output showing Ringdown along with previous data

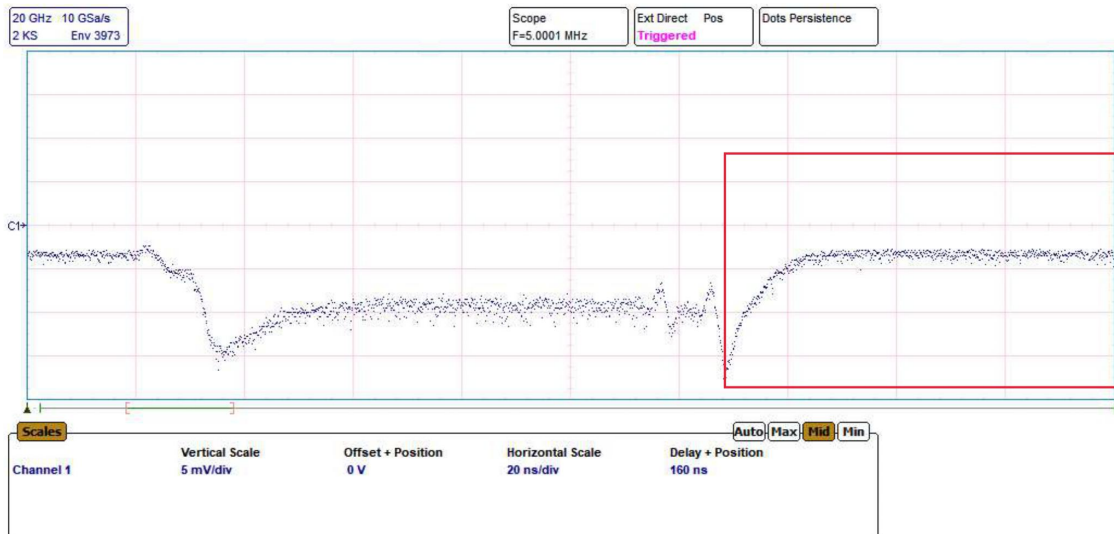


Figure 72: Envelope of the Output for Ringdown calculation

Figure 72 shows a red box, which includes the ringdown time of our resonator at room temperature, we will exponential fit this part to get the ringdown time. The exponential fit of the same is shown in Figure 73. From the fit, ring down time is  $5.495E - 9 \pm 6.81E - 11$ , i.e.,  $5.495 \pm 0.068\text{ns}$ . So, the dead time of the spectrometer is  $5.495 \times 15\text{ ns} = 82.425\text{ ns}$ . So, it is good enough to

conduct the experiment and detect the output signals at room temperature.

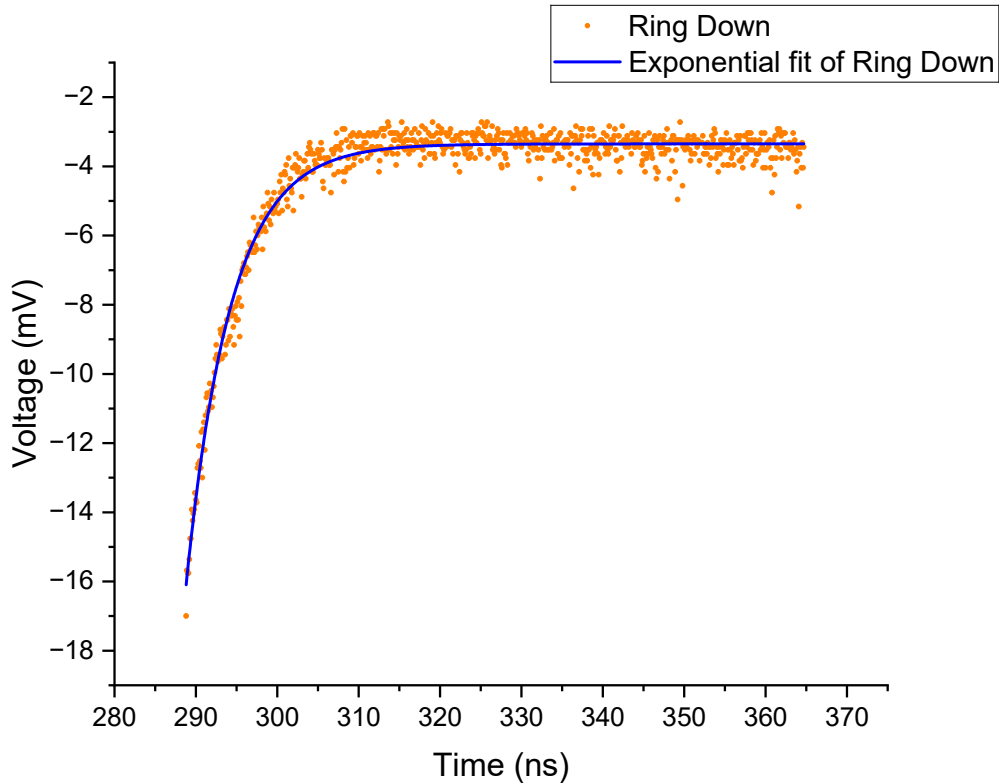


Figure 73: Exponential fit of Red part in Figure 72

The Deadtime on different temperatures we have taken is given in table 2. We can see that dead time at lower temperatures is higher as ringdown time increases with a decrease in temperature, so it is challenging to perform pulsed ESR experiments at very low temperatures with current resonators. So, we will only work on three temperatures: Room, 270K, and 180K.

## 5.5 FID signals of DPPH

We will calculate amplitude from the results from two outputs (code to do so can be found in the appendix). As stated above, we will work on three different

Table 2: Insertion Loss for different number of output ports

Temp.(K)	EM Current (A)	Resonant Frequency (GHz)	Dead time (ns)
Room (297)	11.20	3.325	95
270	11.17	3.3075	100
180	11.02	3.2628	120
90	10.81	3.2053	140
10	10.73	3.1753	170

temperatures in this session. We will also attempt Rabi oscillation at these temperatures. Rabi cycle is the cyclic behaviour of the two-level system in quantum information processing in an oscillatory driving field. We will also calculate the spin relaxation time ( $T_2^*$ ) for each temperature for our DPPH. This is a homodyne experiment, so we don't need to envelope it since it is a DC signal that we are detecting. one example is shown in Figure 74. The signal increase at the start is not data but the time the receiver switch turns on, so we are not interested in that part, but the exponential decay part, which will give us  $T_2^*$ .

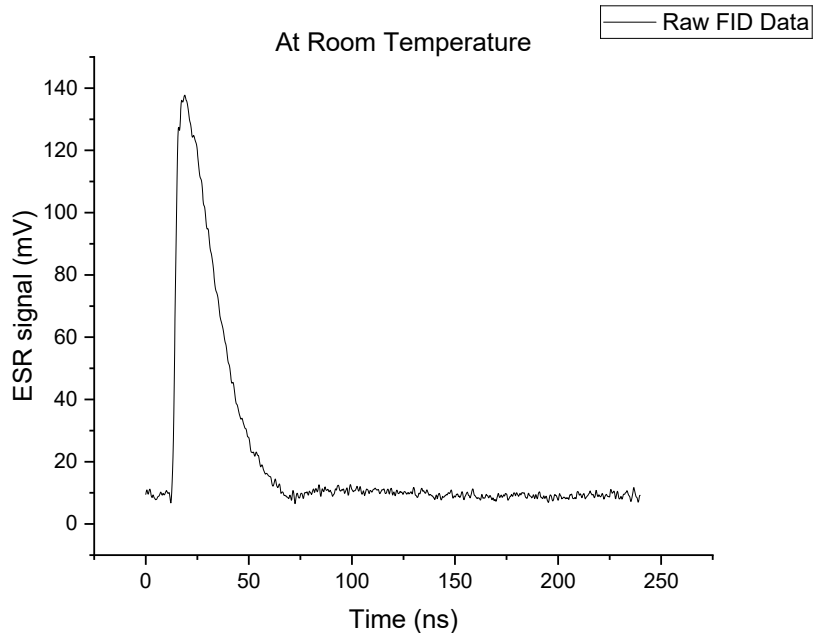


Figure 74: FID (DC) signals detected in the oscilloscope)

### 5.5.1 At Room Temperature

We exponentially fitted the decayed part of the FID envelope of DPPH at this temperature, as shown in Figure 75. So, according to the fit, the spin relaxation time ( $T_2^*$ ) for DPPH at room temperature is 16.58 ns.

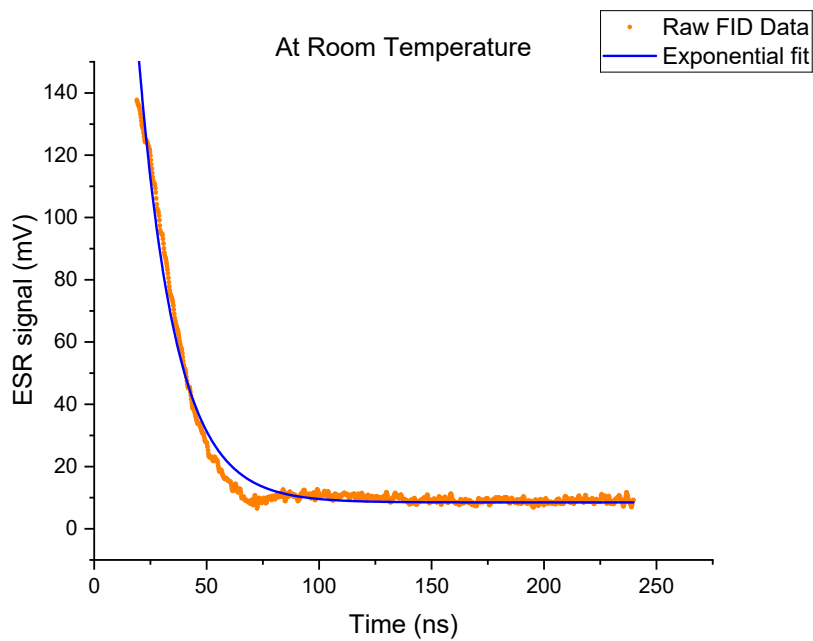


Figure 75: Exponential fit of FID DC signal at Room (297K) temperature

### 5.5.2 At 270K Temperature

We exponentially fitted the decay part of the FID envelope of DPPH at this temperature, as shown in Figure 76. So, according to the fit, the spin relaxation time ( $T_2^*$ ) for DPPH at 270K temperature is 24.93 ns.

### 5.5.3 At 180K Temperature

We exponentially fitted the decay part of the FID envelope of DPPH at this temperature, as shown in Figure 77. So, according to the fit, the spin relaxation

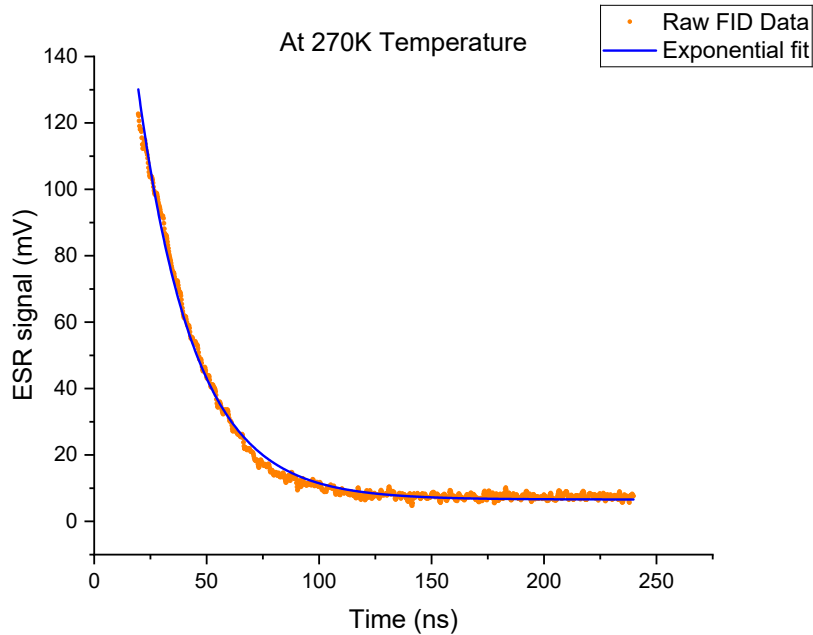


Figure 76: Exponential fit of FID DC signal at 270K temperature

time ( $T_2^*$ ) for DPPH at 180K temperature is 21.22 ns.

## 5.6 Rabi Oscillation

Attempted Rabi oscillation for different temperatures is shown in Figure 78. From the plot, we can conclude that we get an even better Rabi cycle as we go lower in temperature. We observed a complete half cycle at 180K, while we only got part of the half cycle at room temperature. The  $\frac{\pi}{2}$  pulse duration is around 100–130 ns for our experiment, which is slightly different at each temperature.

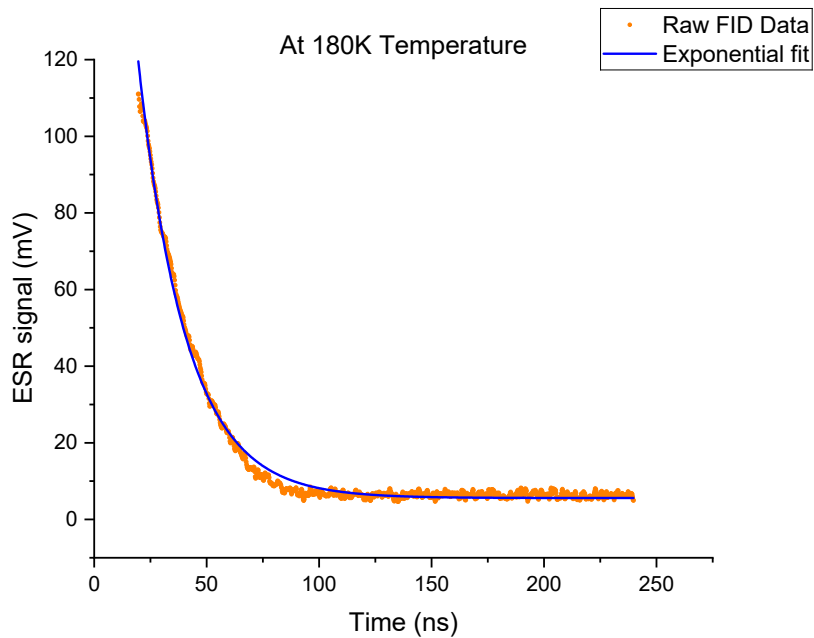


Figure 77: Exponential fit of FID DC signal at 180K temperature

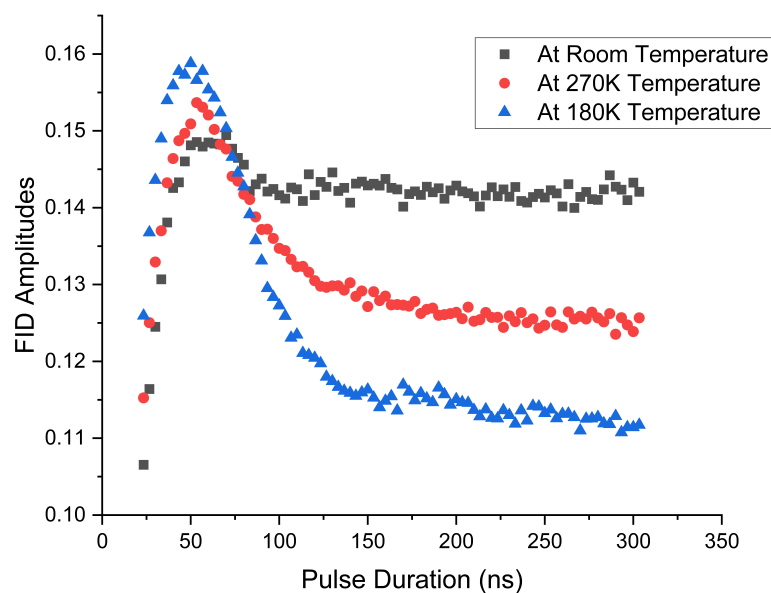


Figure 78: FID amplitudes of DPPH (Attempted Rabi Oscillation) at different temperatures

## Chapter 6

### 6 Future Work

The Rabi oscillation we observed at room temperature, 270K temperature and 180K temperature is not similar to the theoretical trend, but we got a complete cycle at lower temperatures. One can attempt Rabi at a temperature below 100K to get an even better Rabi cycle. One can also try other samples like Galvinoxyl for lower temperatures. One can also make a proper resonator with an even lower Q-factor so that ringdown time is low enough to get an ESR signal at a low temperature.

Although the palette was created, we could not deposit YBCO and test it further to create a resonator due to time constraints. One may try depositing and calculating the Resistance-Temperature plot to get critical temperature. They can make a superconducting resonator that works way better than an ordinary resonator below its critical temperature. One thing to consider is that if one wants to deposit YBCO, one needs an oxygen environment, which will block the Pulsed Laser Deposition chamber for other depositions until it is thoroughly cleaned.

One must also try making a connector of the correct length for the cryostat. This may remove some unwanted reflections that might be coming from the bending of more extended connectors.

## Chapter 7

### 7 Conclusion

We have simulated and fabricated resonators for the sample (DPPH). We have also designed a pulsed electron spin resonance spectrometer, which gives homodyne signals as output rather than traditional heterodyne signals. CW ESR spectrum for our sample was measured.

A Pallete of YBCO was created. R-T was performed on this palette but did not get superconductivity below the critical temperature. As a result, further calculations are done using an omega resonator.

We have performed a pulsed electron spin resonance experiment on the DPPH sample. FID signals at different temperatures have been measured. The calculated spin relaxation time ( $T_2^*$ ) of DPPH at room temperature is 16.58 ns, at 270K temperature is 24.93 ns and at 180K temperature is 21.22 ns. Attempted Rabi oscillation is measured. It was found that as we go lower in temperature, we get an even better Rabi cycle (as we got a complete half cycle for 180K but only got part of a half cycle for room temperature). Our experiment uses the  $\frac{\pi}{2}$  pulse duration of 100-130 ns.

## Appendix A

### Python code for remote oppression of CW ESR using VNA and power supply of electromagnet

```
import pyvisa as visa
import time as t
import matplotlib.pyplot as plt

rm=visa.ResourceManager()
dev='TCPIP0::10.20.93.11::9221::SOCKET'
sup=rm.open_resource(dev)
sup.read_termination='\r\n'
sup.write_termination='\r\n'

rm1=visa.ResourceManager()
dev1='TCPIP0::10.20.103.75::inst0::INSTR'
vna=rm.open_resource(dev1)
vna.read_termination='\n'
vna.write_termination='\n'

#print(vna.query("*IDN?"))

sup.write('SOUR:VOLT 20.0')
```

```
sup.write('SOUR:CURR 10.0')

start=2E9
stop=5E9
start=str(start)
stop=str(stop)

vna.write("SYSTem:DISPlay:UPDAtE ON")

vna.write("MEM:DEF 'k1'")

vna.write('SENS1:FREQ:STAR '+start)
vna.write('SENS1:FREQ:STOP '+stop)

vna.write("CALC2:PAR:SDEF 'Trc2', 'S11'")
vna.write("DISP:WIND2:STAT ON")
vna.write("DISP:WIND2:TRAC:FEED 'Trc2'")

vna.write("CALC2:MARK1 ON")
t.sleep(5)

n=51
im=10
iM=20
lst=[]
```

```
for i in range(n):
    curr=float(im+(i*(iM-im)/(n-1)))
    i_str=str(curr)
    sup.write('SOUR:CURR '+i_str)

    t.sleep(5)

    vna.write("CALC2:MARK1:FUNC:EXEC MIN")

    res=vna.query("CALC2:MARK1:FUNC:RES?")
    print(i,i_str,res)

    r=res.split(",")
    #print(r)

    lst.append([i,curr,float(r[0]),float(r[1])])

    #print(lst)

    sup.write('SOUR:VOLT 0.0')
    sup.write('SOUR:CURR 0.0')

    #vna.write("MEM:DEL 'k1'")

A=[[0 for x in range(n)] for y in range(4)]
```

```
for i in range(n):
    for j in range(4):
        A[j][i] = lst[i][j]

#print(A)

plt.plot(A[1],A[3])
plt.xlabel("Current")
plt.ylabel("S11")
plt.show()
```

## Python code for recording and processing oscilloscope output in Pulsed ESR spectrometer

```
from spinapi import *
import time as ti
import numpy as np
import pyvisa as visa
import matplotlib.pyplot as plt
import re
# Enable the log file
#pb_set_debug(0)

rm=visa.ResourceManager()
osci=rm.open_resource("TCPIPO::192.168.0.110::inst0::INSTR")
```

```
osci.read_termination="\n"
osci.write_termination="\n"

pb_select_board(0)

if pb_init() != 0:
    print("Error initializing board: %s" % pb_get_error())
    input("Please press a key to continue.")
    exit(-1)

# Configure the core clock
pb_core_clock(300)

osci.write("FORM ASC")
osci.write("CHAN1:DATA:POIN DMAX")
osci.write("CHAN2:DATA:POIN DMAX")
osci.write("STOP")

# Program the pulse program
time_base=10/3
start_n=7
stop_n=91

start_tp=start_n*time_base
stop_tp=stop_n*time_base
```

```

durations=np.linspace(start_tp,stop_tp,stop_n-start_n+1)
#durations=[30,60,100]
print(durations)
dead_time=95
N_avg=1
N=20
T_s=float(osci.query("CHAN1:DATA:XINC?"))
for it in range(N):
    print(it)
    for i in durations:
        #print(i)
        pb_start_programming(PULSE_PROGRAM)
        start = pb_inst_pbonly(0b00000000000000000000000011011, CONTINUE, 0, i* ns)
        pb_inst_pbonly(0b00000000000000000000000000000000, CONTINUE, 0, dead_time * ns)
        pb_inst_pbonly(0b000000000000000000000000100100, CONTINUE, 0, 600.0 * ns)
        pb_inst_pbonly(0b00000000000000000000000000000000, BRANCH, start, 100.0 * ns)
        pb_stop_programming()
        pb_reset()
        pb_start()

        ti.sleep(0.5)

a=[]
for j in range(N_avg):
    # osci.write("RUN")
    # ti.sleep(0.05)

```

```
# osci.write("STOP")

osci.write("SINGLE")
ti.sleep(0.5)

fid_str=osci.query("CHAN1:DATA?")
#print(fid_str)

fid_signal=[float(i) for i in fid_str.split(',')]

fid_sq=np.power(fid_signal,2)

fid_str1=osci.query("CHAN2:DATA?")
#print(fid_str)

fid_signal1=[float(i) for i in fid_str1.split(',')]

fid_sq1=np.power(fid_signal1,2)

time=np.multiply(list(range(0, len(fid_sq))),T_s)

#plt.plot(time,np.sqrt(fid_sq+fid_sq1))

if(j==0):
    a=np.sqrt(fid_sq+fid_sq1)
else:
    a+=np.sqrt(fid_sq+fid_sq1)

#plt.show()

a=a/N_avg

time=np.multiply(list(range(0, len(fid_sq1))),T_s)

#plt.plot(time,a)
```

```
#plt.show()

with open("RABI_seq"+str(i)+"-"+str(it)+".txt","w+") as f:
    for i in range(len(time)):
        f.write(str(time[i])+"\t"+str(a[i])+"\n")

\Psi\Psi

# Trigger the board

#time.sleep(10)

#pb_stop()
#pb_close()
```

## References

- [1] Spectrometry as a non-destructive technique in identifying cultural archaeological heritage. In Eman Osman, editor, *Spectroscopic Techniques for Archaeological and Cultural Heritage Research*, 2053-2563, pages 1–1 to 1–11. IOP Publishing, 2020.
- [2] F. Bloch and A. Siegert. Magnetic resonance for nonrotating fields. *Phys. Rev.*, 57:522–527, Mar 1940.
- [3] Dimitar Dimitrov, Kristiaan Schreve, A. Taylor, and B. Vincent. Rapid prototyping driven design and realisation of large components. *Rapid Prototyping Journal*, 13:85–91, 04 2007.
- [4] G Donaldson, R Bowman, A Cochran, Katherine Kirk, Colin Pegrum, and J Macfarlane. Progress in high  $t_c$  magnetic sensors and their applications. *Physica Scripta*, 1992:34, 01 2007.
- [5] Ziad Dughaish. Effect of annealing and addition of fine metal powders on the mechanical properties of  $\text{YBa}_2\text{Cu}_3\text{O}_7$  high temperature superconductor (hts). 01 2016.
- [6] S.S. Eaton, G.R. Eaton, and L. Berliner. *Biomedical EPR - Part B: Methodology, Instrumentation, and Dynamics*. Biological Magnetic Resonance. Springer US, 2006.
- [7] John McCracken. Electron paramagnetic resonance: A practitioner's toolkit. *Journal of the American Chemical Society*, 131(36):13181–13181, 2009. PMID: 19702263.

- [8] Subhadip Roy, Anuvab Nandi, Pronoy Das, and Chiranjib Mitra. S-band electron spin resonance spectroscopy using a short-circuited coplanar waveguide resonator. *IOP SciNotes*, 1:035202, 11 2020.
- [9] Subhadip Roy, Anuvab Nandi, Pronoy Das, and Chiranjib Mitra. Detection of electron spin resonance down to 10 k using localized spoof surface plasmon. *Journal of Physics D: Applied Physics*, 54, 05 2021.
- [10] Subhadip Roy, Sagnik Saha, Jit Sarkar, and Chiranjib Mitra. Development of planar microstrip resonators for electron spin resonance spectroscopy. *The European Physical Journal Applied Physics*, 90:31001, 06 2020.
- [11] J. Stolze and D. Suter. *Quantum Computing: A Short Course from Theory to Experiment*. Wiley, 2008.
- [12] Xiangxia Wei, Ragavendran Sundaram Nagarajan, Erwin Peng, Junmin Xue, John Wang, and Jun Ding. Fabrication of yba<sub>2</sub>cu<sub>3</sub>o<sub>7-x</sub> (ybco) superconductor bulk structures by extrusion freeforming. *Ceramics International*, 42(14):15836–15842, 2016.
- [13] J.A. Weil and J.R. Bolton. *Electron Paramagnetic Resonance: Elementary Theory and Practical Applications*. Wiley, 2007.